Research Article

A Novel Pyroptosis-Based Prognostic Model Correlated with the Parainflammatory Immune Microenvironment of Pancreatic Cancer

Kong-kong Wei (ID),[1] **Zhi-xing Du** (ID),[1] **Jun-ge Deng** (ID),[1] **Jin-wei Yang** (ID),[1] and **Hao Chen** (ID)[1,2]

[1]*Department of Surgical Oncology, Lanzhou University Second Hospital, No. 82 Cuiyingmen Road, Chengguan District, Lanzhou 730030, China*
[2]*Key Laboratory of Digestive System Tumors of Gansu Province, Lanzhou University Second Hospital, No. 82 Cuiyingmen Road, Chengguan District, Lanzhou 730030, China*

Correspondence should be addressed to Hao Chen; ery_chenh@lzu.edu.cn

Background. Pyroptosis has a dual function in malignant tumor progression and management. The action of pyroptosis-related genes (PRGs) in pancreatic cancer (PC), however, remains uncertain. *Methods.* Differential expression analyses of 57 PRGs were conducted in the TCGA TARGET GTEx dataset. The candidate genes were determined using LASSO Cox regression and random forest analyses. A risk model was developed with the TCGA dataset and validated with the ICGC dataset. *Results.* Three prognosis-related PRGs (BAK1, GSDMC, and IL18) were chosen to create a risk model. High-risk patients from the TCGA and ICGC cohorts had an unfavorable overall survival (all $p < 0.05$). The risk model's accuracy and independent predictability were assessed by receiver operating characteristic curves and multivariate Cox regression analysis, respectively. High-risk patients possessed different molecular pathways, higher KRAS and TP53 mutations, increased expression of PD-L1, C1 immune subtype, and immuno-suppressive microenvironment characterized by parainflammation compared to low-risk patients. KRAS and TP53 mutations participated in different inflammatory pathways and played different prognostic roles between the two risk groups. KRAS mutations in high-risk patients caused a more unfavorable prognosis than wild-type KRAS ($p = 0.016$), whereas TP53 mutations in low-risk patients exhibited a poorer outcome than wild-type TP53 ($p = 0.009$). Spearman correlation analyses revealed that the parainflammatory response in PC might be implicated in GSDMC-mediated pyroptosis via cytosolic DNA-sensing pathways under hypoxic conditions. Furthermore, the risk scores were significantly and positively related to the expression of HNRNPC, RBM15, YTHDF1, and YTHDF2, as well as sensitivity to gemcitabine, cisplatin, and erlotinib. *Conclusions.* This study created a novel pyroptosis-based risk model related to the parainflammatory immune microenvironment, which might help identify novel biomarkers, evaluate the tumor immune microenvironment, and develop management strategies for PC patients.

1. Introduction

Pancreatic cancer (PC) remains one of the most lethal malignancies worldwide. The disease ranks the fourth most common cancer-related death among both sexes in the United States [1] and sixth in China [2]. There were an estimated 458,918 new cases of PC diagnosed and 432,242 deaths from the disease globally in 2018 [3]. PC, a highly aggressive tumor, had a dismal prognosis [1]. Most PCs (more than 90%) are pancreatic ductal adenocarcinomas (PDACs) [4]. Surgical resection is regarded as the only potentially curative treatment for PC patients [5], but unfortunately, the majority of patients are either diagnosed at a late stage or are frequently ineligible for surgery, resulting in less than 20% of patients undergoing an operation [6]. Besides, even after radical resection, patients with PC are likely to experience high local recurrence rates and often have distant metastases [7]. Systemic chemotherapies are currently the standard regimen for treating advanced or metastatic PC, offering a slight overall survival (OS) benefit of only months [8, 9]. Immune therapy has been a hot topic in PC studies, but single-agent immune checkpoint inhibitors (ICIs) have generally been

proven to be ineffective in clinical trials [10]. The immuno-suppressive microenvironment is considered to cause PC resistance to immune therapies [11]. At present, the prognostic prediction of PC is mainly dependent on the clinico-pathological staging system, which lacks accurate guidance for the prognosis and treatment of PC. Therefore, identifying novel predictive biomarkers for estimating the immune microenvironment is critically essential to predict survival and lay down personalized treatment regimens for PC patients.

Programed cell death (PCD), which is modulated by specific signaling pathways, is essential in maintaining homeostasis, host defense, cancer, and other pathologies [12]. PCD has been categorized into several distinct types, including apoptosis, autophagy, necrosis, ferroptosis, and pyroptosis [13]. Pyroptosis, different from other types of PCD, is generally regarded as a highly pro-inflammatory form of PCD [14]. Pyroptosis was observed for the first time in 1986 in mouse macrophages [15]. But until 2001, the first definition of pyroptosis introduced by Cookson and Brennan [16] distinguished it from apoptosis. In 2018, pyroptosis was described as a regulated cell death, which is mainly dependent on cytoplasmic membrane pore formation executed by gasdermin family members and is commonly (but not always) induced by inflammatory caspase activation [17].

Pyroptosis may be triggered by inflammasomes or without inflammasomes. Pyroptosis pathways dependent on inflammasomes comprise canonical caspase-1 pathway and noncanonical caspase-4/5/11 pathway, whereas inflammasome-independent pathways consist of granzyme proteases-dependent pathway and caspase-3-dependent pathway [18]. The canonical inflammasomes are started by pathogens or damage, which recruits pro-caspase-1 through inflammasome adaptor protein ASC (also called PYCARD), causing its self-cleavage and activating caspase-1 [19, 20]. Caspase-1 activation can mature pro-IL-1 and pro-IL18 [21] and cleave gasdermin D (GSDMD) protein to produce the GSDMD-N domain that forms the membrane pore to facilitate the release of IL-1β and IL18 [22]. The noncanonical pathway involves the activation of pro-caspase-4/5/11 [23–25] to cleave GSDMD [26] and trigger pyroptosis. Activated caspase-11 induces NLRP3 inflammasome to start caspase-1, which promotes the maturation of IL-1β and IL18 [27, 28]. In the inflammasome-independent pathways, activated caspase-3 by chemotherapeutic drug cleaves gasdermin E (GSDME) into its N-terminal domain, causing cell membrane pores to form [29, 30]. In the granzyme proteases mediated pathway, the granzyme B produced by T cells or natural killer cells (NKs) leads to the target cell pyroptosis by direct cleavage of GSDME [31, 32].

Despite numerous recent studies exploring the functions of pyroptosis in cancers, it remains ambiguous how pyroptosis affects cancer prognosis and treatment. The reason for this may be the dual function of pyroptosis in cancer progression and management. Pyroptosis activation and cytokine release modify the tumor immune microenvironment (TIME) and facilitate tumor progression via evading immunosurveillance and inducing immune tolerance. Pyroptosis, however, can also improve immunotherapies through recruiting and activating immune cells to kill tumor cells [33, 34]. In some tumor types, including hepatocellular carcinoma [35], lung adenocarcinoma [36], and bladder cancer [37], pyroptosis-related genes (PRGs) have been assessed for their impact on prognosis and TIME. In PC, the functions of PRGs remain unclear and need to be further investigated. Hence, a novel pyroptosis-based risk model was established in the current study. We systematically explored the association of the risk model with prognosis, signaling pathways, somatic mutation, m6A-related gene expression, TIME, and drug sensitivity in PC. In addition, Increasing evidence demonstrates that pyroptosis is involved in inflammation and cancer immunity, but little is known about its correlation with parainflammation. Therefore, this study investigated and discussed the potential mechanisms of the influence of parainflammation on pyroptosis and TIME in PC. We found that cytosolic DNA-sensing pathways might participate in parainflammation-induced pyroptosis, which, to our knowledge, has not been reported previously.

2. Materials and Methods

2.1. Data Collection and Preprocessing. Since the TCGA dataset lacks sufficient data on normal pancreatic tissues, we downloaded the TCGA TARGET GTEx dataset ($n = 19,109$) with the Toil RNA-seq recompute expected_count version (accessed on November 19, 2021) from the UCSC Xena database [38]. Gene expression levels were presented as log2 (expected_count + 1). mRNA expression data for PC were derived from the TCGA TARGET GTEx dataset to determine differentially expressed PRGs. Data on 182 PC patients, including clinical information, RNA sequencing expression, and somatic mutations, were acquired from the TCGA database (accessed on December 4, 2021) as a training set. Eighty-two PC patients' gene expression and clinicopathological data were available from the ICGC database (accessed on December 1, 2021) as a validation cohort. The transcripts per million (TPM) values for the TCGA and ICGC cohorts were converted from the fragments per kilobase of transcript per million mapped reads (FPKM) values according to the algorithm reported in previous studies [39, 40]. The TPM values were utilized for the subsequent analysis. The flow of our work is exhibited in Figure 1. Furthermore, 57 genes (*Supplementary 1*) associated with pyroptosis were collected from both a previous study [41] and the Molecular Signatures Database (MSigDB) [42].

2.2. Identifying Differentially Expressed PRGs. Differentially expressed genes (DEGs) in pancreatic tumor tissues and nontumor tissues from the TCGA TARGET GTEx cohort were analyzed using "DESeq2," "edgeR," and "limma" R packages with a threshold false discovery rate < 0.05 and $|\log2FC| \geq 1$. The intersection analysis of the three DEG sets obtained by the above methods found shared upregulated and downregulated DEGs. Subsequently, the intersection of PRGs with shared upregulated and downregulated DEGs identified differentially expressed PRGs for further analysis.

2.3. Constructing and Validating a Risk Model. Based on the STRING database (version 11.5) [43], an interaction network of the differentially expressed PRGs in the TCGA cohort was
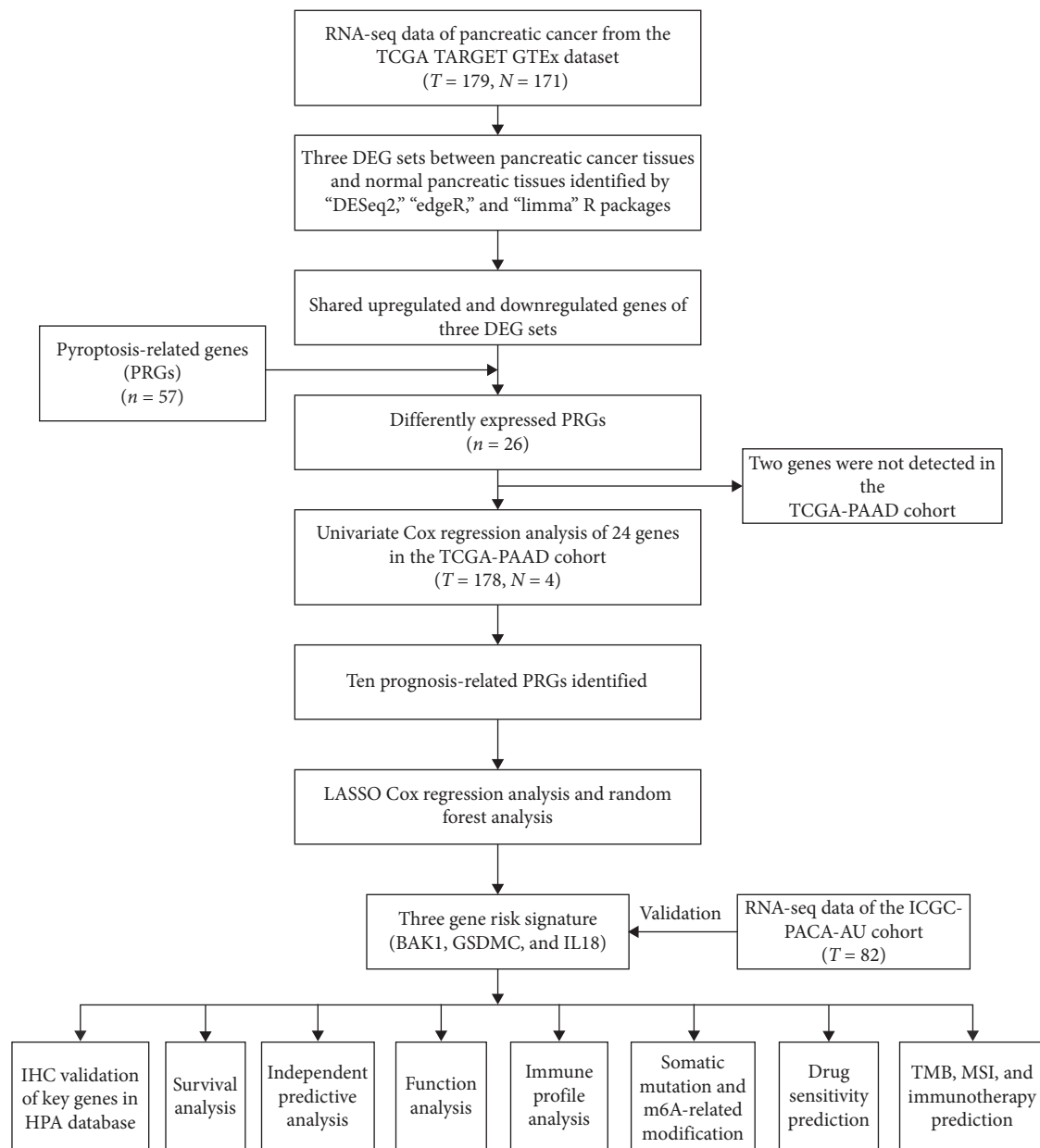
FIGURE 1: Flowchart of the current study. PRGs, pyroptosis-related genes; DEGs, differentially expressed genes; T, tumor; N, normal; IHC, immunohistochemistry; HPA, Human Protein Atlas database; TMB, tumor mutation burden; MSI, microsatellite instability.

constructed. Using the R packages "igraph" and "reshape2," a correlation network was created for candidate genes. Univariate Cox analysis using the "Survival" R package assessed the prognostic value of differentially expressed PRGs in the TCGA cohort. Least absolute shrinkage and selection operator (LASSO) Cox regression analysis ("glmnet" R package) and random forest analysis ("randomForestSRC" R package) were performed in the TCGA cohort to screen out candidate genes. The shared genes obtained by these two methods were selected as final signature genes to construct a risk model. Immunohistochemical (IHC) staining data for signature genes were obtained from the Human Protein Atlas (HPA) database. The expression levels of each of

the signature genes and the corresponding exponentiated regression coefficients of the multivariate Cox regression model were used to compute PC patient risk scores.

The median risk score divided the patients into low- and high-risk groups. The "stats" and "Rtsne" R packages were used for principal component analysis (PCA) and t-distribution stochastic neighborhood embedding analysis (t-SNE), respectively. A Kaplan–Meier analysis with a log-rank test compared the OS between two risk groups. To investigate whether risk scores independently predicted patient prognosis, the risk score and clinicopathological features were analyzed with univariate and multivariate Cox regression analyses. Clinicopathological

characteristics of both risk groups were compared using the χ^2 test and presented as a heat map, including gender, age, TNM stage, T stage, N stage, M stage, and histological grade. The predictability of clinicopathological characteristics and the risk signature for 1-, 2-, and 3-year survival rates was estimated in the TCGA and ICGC cohorts using receiver operating characteristic (ROC) curves.

2.4. Function Analysis. Gene set enrichment analysis (GSEA) is a computational method for evaluating the distributional trend of a predefined gene set in the gene table ordered according to phenotypic relevance, thereby determining its impact on the phenotype [44]. The TCGA cohort was analyzed using GSEA to identify underlying pathways between the high- and low-risk groups. MsigDB provided KEGG gene sets (c2.cp.kegg.v7.4.symbols.gmt) and GO gene sets (c5.go.v7.4.symbols.gmt) as the reference gene sets to perform GSEA analysis. Determination of significance was performed with $p < 0.05$ as the screening threshold. The gene sets of hypoxia (HALLMARK_HYPOXIA.v7.5.1.gmt) and the cGAS-STING pathway (REACTOME_STING_MEDIATED_INDUCTION_OF_HOST_IMMUNE_RESPONSES.v7.5.1.gmt) were also derived from MSigDB. The gene sets of the NF-kappaB pathway and the tumor necrosis factor (TNF) signaling pathway were acquired from a previous study [45]. To obtain enrichment scores for each pathway in each sample, single-sample GSEA (ssGSEA) scores for these four gene sets were computed using the gene set variation analysis (GSVA) package [46].

2.5. Immune Profile. The immune infiltration in tumor tissues was assessed with online tools and bioinformatics algorithms. TIMER2.0 provides users with multiple immune deconvolution methods, including XCEL, TIMER, QUANTISEQ, MCPCOUNTER, EPIC, CIBERSORT, and CIBERSORT-ABS algorithms [47]. The relationship of the risk score with immune infiltrating cells was evaluated using Spearman correlation analysis. Employing the Wilcoxon test in the R package "ggpubr," we compared ssGSEA scores between the two risk groups for 14 immune-related pathways, including 13 pathways reported in a previous study [48] and the cGAS-STING pathway engaged in the induction of host immune responses. There may be an association between immune checkpoint gene expression and the efficacy of ICIs. Therefore, 47 immune checkpoint genes (Supplementary 1) were extracted from the training set and compared between the two risk groups. Moreover, we detected the association between the risk scores and six immune subtypes (C1–C6), namely C1 (wound healing), C2 (interferon (IFN)-gamma dominant), C3 (inflammatory), C4 (lymphocyte depleted), C5 (immunologically quiet), and C6 (TGF-beta dominant) [49].

2.6. Somatic Mutation and m6A-Related Modification Analyses. The mutation annotation format of somatic variants was available from the TCGA database, and visualization was done via the R package "maftools." The somatic mutation count in the two risk groups was compared. In addition, we explored the effect of m6A-related modification on the risk signature by analyzing gene expression differences of m6A RNA methylation regulators between different risk groups.

2.7. Drug Sensitivities. The sensitivity of PC patients to targeted agents chemotherapeutic agents was assessed using the "pRRophetic" package [50], which predicts the half-maximal inhibitory concentration (IC_{50}) of selected agents in both high- and low-risk groups. CellMiner database [51] was utilized to evaluate the association of individual prognostic genes with drug sensitivity. We extracted FDA-approved drugs from this database. An analysis of Pearson correlation was conducted with a screening threshold of $p < 0.05$.

2.8. Tumor Mutation Burden, Microsatellite Instability, and Immunotherapy. Data on the tumor mutation burden (TMB) and microsatellite instability (MSI) were obtained from the TCGA cohort through "maftools" and TCGAbiolinks" [52] R packages, respectively. Based on the reported dataset comprising 47 melanoma patients who had received ICIs therapy [53], we used the Subclass Mapping method [54, 55] to predict the response of different risk groups to ICIs treatment, including CTLA-4 and PD-1 inhibitors.

2.9. Statistical Analysis. All statistical analyses and data visualization were performed using R software (Version 4.1.0). Chi-square tests were employed to compare the different proportions of categorical variables. The Wilcoxon rank-sum tests and the Kruskal–Wallis test were utilized to compare two and multiple groups of nonnormally distributed continuous variables, respectively. Spearman correlation analysis was used to evaluate the correlations of the risk score with immune infiltrating cells and construct a Spearman correlation heatmap. The association of three prognosis-related PRGs expressions with drug sensitivity was assessed via Pearson correlation analysis. Two-tailed P values less than 0.05 were statistically significant in all statistical results.

3. Results

3.1. Identifying Differentially Expressed PRGs. In total, 5,241 upregulated genes and 2,884 downregulated genes, 5,182 upregulated genes and 2,941 downregulated genes, and 3,737 upregulated genes and 4,072 downregulated genes were identified between pancreatic tumor tissues and nontumor tissues of the TCGA TARGET GTEx cohort using "Deseq2," "edgeR," and "limma" packages, respectively (Figure 2(a)). Then, we obtained 6,494 DEGs shared by the above three methods, including 3,704 shared upregulated genes (Figure 2(b)) and 2,790 shared downregulated genes (Figure 2(c)). Twenty-six differently expressed PRGs were acquired by computing the intersection of 57 PRGs with 6,494 DEGs (Figure 2(d)). These 26 genes differently expressed between tumor and normal tissues were presented as a heatmap plot, with most of them highly expressed in PC tissues (Figure 2(e)). Except for two genes (CAPS5 and NLRP7), 24 of the 26 differentially expressed PRGs in the TCGA cohort were extracted for further analysis. A protein–protein interaction (PPI) analysis was performed for these 24 genes using the STRING database, as shown in Figure 2(f). In Figure 2(g), a correlation network was constructed between the 24 genes.
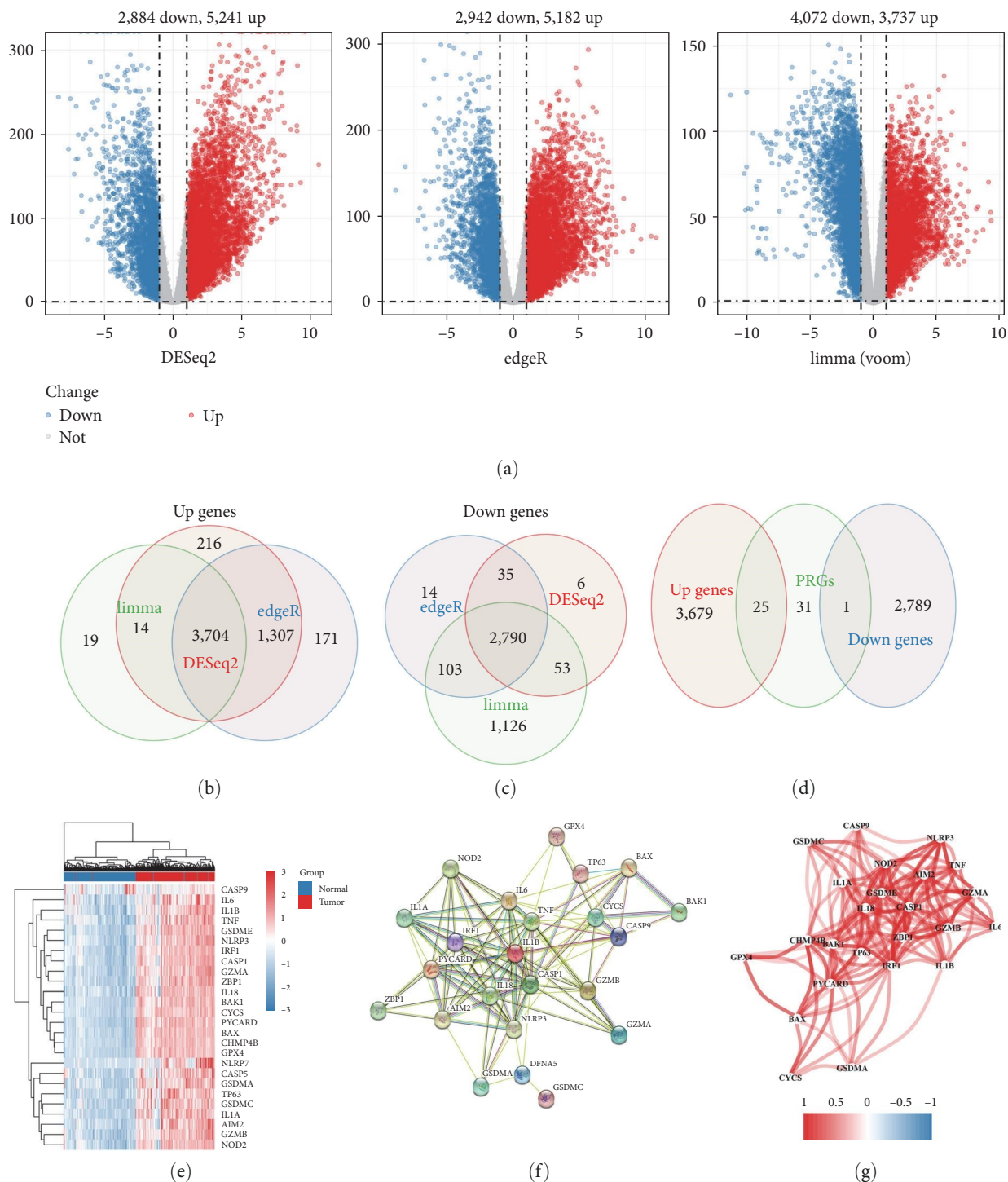
FIGURE 2: Differentially expressed PRG identification: (a) volcano plots of three DEG sets identified in TCGA TARGET GTEx dataset using "DESeq2," "edgeR," and "limma" R packages; (b) Venn plot of upregulated genes shared by three DEG sets; (c) Venn plot of downregulated genes shared by three DEG sets; (d) Venn plot of the intersection of PRGs with shared upregulated and downregulated DEGs; (e) heatmap of 26 differently expressed PRGs. Red and blue represent high and low levels of expression, correspondingly; (f) the PPI network of 24 PRGs with differential expression from the STRING database; (g) the correlation plot of 24 PRGs with differential expression in the TCGA-PAAD cohort. Red and blue signify positive and negative correlations, respectively. PPI, protein–protein interaction.

3.2. Constructing a Risk Signature. We used the TCGA-PAAD cohort as the training cohort to create a prognostic risk signature. A total of 177 PC samples with survival data were included in the survival analysis. A preliminary screening of prognosis-related genes was performed by univariate Cox regression analysis. Among the 24 differentially expressed PRGs, 10 genes significantly related to patient survival (HRs > 1 for all 10 genes) were selected for further study (Figure 3(a)). The LASSO Cox regression analysis identified four genes (BAK1, GSDMC, IL18, and TP63) by the optimum λ value (Figures 3(b) and 3(c)). Besides, we performed random forest analysis and screened out three genes (BAK1, GSDMC, and IL18) using a minimal depth approach (Figures 3(d) and 3(e)). Finally, three shared genes (BAK1, GSDMC, and IL18) of these two gene lists were retained as signature genes (Figure 3(f)). Significantly increased mRNA expression levels of these three signature genes were found in PC tissues compared to normal pancreatic tissues (Figure 2(e)). We further assessed the protein expressions of three signature genes in the HPA database and found that BAK1 and IL18 were overexpressed in PC tissues, whereas no GSDMC protein expression was observed in PC or normal tissues (*Supplementary 2*).

A three-gene prognostic signature was built according to the results of multiple Cox regression analysis, and each patient's risk score was computed using the formula: the risk score = (1.496 × expression level of BAK1) + (1.255 × expression level of GSDMC) + (1.336 × expression level of IL18). The median risk score categorized PC patients into two groups: the high-risk group ($n = 88$) and the low-risk group ($n = 89$). An obvious correlation between the patients' risk scores and the probability of death was observed, as evidenced by the distribution of risk scores and survival status (Figures 4(a) and 4(b)). PCA and t-SNE analyses confirmed that high- and low-risk patients were distributed in distinct directions (Figures 4(c) and 4(d)). Kaplan–Meier survival analysis demonstrated that high-risk patients had a significantly more dismal prognosis compared to the low-risk patients ($p = 0.047$) (Figure 4(e)). The predictive accuracy of the risk signature was evaluated by time-dependent ROC curves, and the results indicated areas under the curve (AUC) values of 0.681, 0.641, and 0.701 for 1-, 2-, and 3-year survival, respectively (Figure 4(f)).

3.3. Validating the Risk Signature. The ICGC-PACA-AU dataset as external verification data further confirmed the robustness of the three gene signatures constructed in the TCGA dataset. In the same way, the calculation of risk scores for each patient in the ICGC-PACA-AU cohort was based on the expression levels of three signature genes and their exponentiated regression coefficients. The classification of the cases into the high- and low-risk groups was performed using the median risk score of the cohort. Similarly, death rates rose with higher risk scores (Figures 5(a) and 5(b)). Also, PCA and t-SNE analyses validated the risk score's ability to classify (Figures 5(c) and 5(d)). According to Kaplan–Meier survival curves (Figure 5(e)), high-risk patients exhibited a decreased survival rate when compared to low-risk patients ($p = 0.045$). The AUC values for the risk signature at 1, 2, and 3 years were 0.597, 0.631, and 0.694, respectively (Figure 5(f)).

3.4. Independent Predictive Capability of the Risk Score. The available variables for the TCGA-PAAD cohort were assessed using univariate and multivariate Cox regression analyses to ascertain whether the risk score could independently predict patient prognosis. The results indicated that the risk score was significantly related to OS in both univariate and multivariate Cox regression analyses (hazard ratio (HR) = 1.225, 95% confidence interval (CI): 1.117–1.343, $p < 0.001$; HR = 1.214, 95% CI: 1.098–1.342, $p < 0.001$, respectively) (Figures 6(a) and 6(b)). We also evaluated the associations of clinicopathological characteristics with the risk score, and the heatmap result showed a significant difference in histological grade between the two risk groups. Moreover, the three PRGs (BAK1, GSDMC, and IL18) were significantly overexpressed in the high-risk group as compared to the low-risk group. Nevertheless, no significant difference was found in the clinicopathological factors such as age, gender, T stage, N stage, M stage, and TNM stage between the two risk groups (Figure 6(c)). The time-dependent ROC curve depicted the 1-year AUC value of 0.681 for the risk score, and it exhibited superior predictive ability over clinicopathological characteristics (Figure 6(d)).

3.5. Function Analysis. The GSEA analysis of the TCGA cohort identified the underlying biological processes and enrichment pathways relevant to the risk model by analyzing GO terms and KEGG pathways. The top 5 KEGG pathways and GO terms were determined according to the p-value- < 0.05. Based on the results of the GSEA analysis, the enriched KEGG pathways and GO terms in the high-risk group were mostly correlated with drug metabolism signaling pathways (drug metabolism-other enzymes) as well as tumor-related biological processes and signaling pathways, including cell cycle, P53 signaling pathway, DNA replication, pathways in cancer, mitotic nuclear division, epidermal cell differentiation, mitotic sister chromatid segregation, and epidermis development (Figures 7(a) and 7(c)), whereas the enriched KEGG pathways and GO terms in the low-risk group were mainly engaged in other pathways and biological processes, such as calcium signaling pathway, neuroactive ligand–receptor interaction, regulation of membrane potential, peptide hormone secretion, regulation of neurotransmitter level, and so on (Figures 7(b) and 7(d)). These findings suggested that PRGs associated with prognosis are probably involved in the drug treatment, occurrence, and progression of PC.

3.6. Immune Profile Analysis. Spearman correlation analysis was made to investigate the association of the risk score with immune infiltration using different algorithms, as depicted in Figure 8(a). According to the results, most of the immune cells, including B cells, Th2 CD4+ T cells, CD8+ T cells, regulatory T (Treg) cells, follicular helper T cells, neutrophils, M0 macrophages, M1 macrophages, M2 macrophages (from the CIBERSORT-ABS algorithm), NK cells, cancer-associated fibroblasts (CAFs), and myeloid dendritic cells (mDCs) (from the TIMER, CIBERSORT, and CIBERSORT-ABS algorithms) had a positive relation with the risk score. The ssGSEA scores of 14 immune-related pathways were calculated
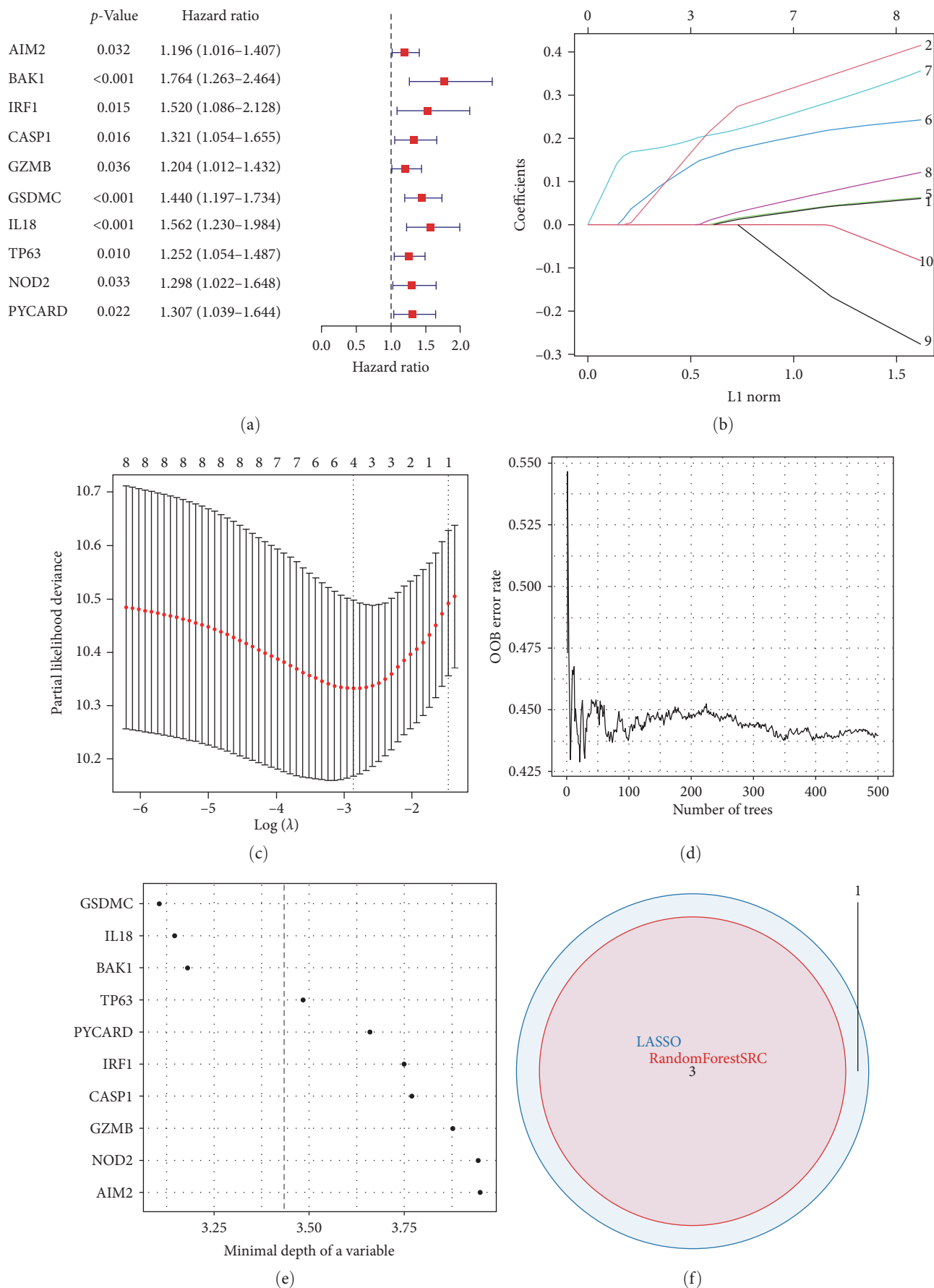
FIGURE 3: Constructing a risk signature in the TCGA cohort: (a) forest plot of 10 prognostic-associated PRGs identified by univariate analysis based on $p < 0.05$; (b, c) 10 prognosis-associated PRGs were subjected to LASSO Cox regression analysis; (d, e) random forest analysis of 10 prognosis-related PRGs; (f) Venn plot of the shared genes between LASSO Cox regression analysis and random forest analysis.
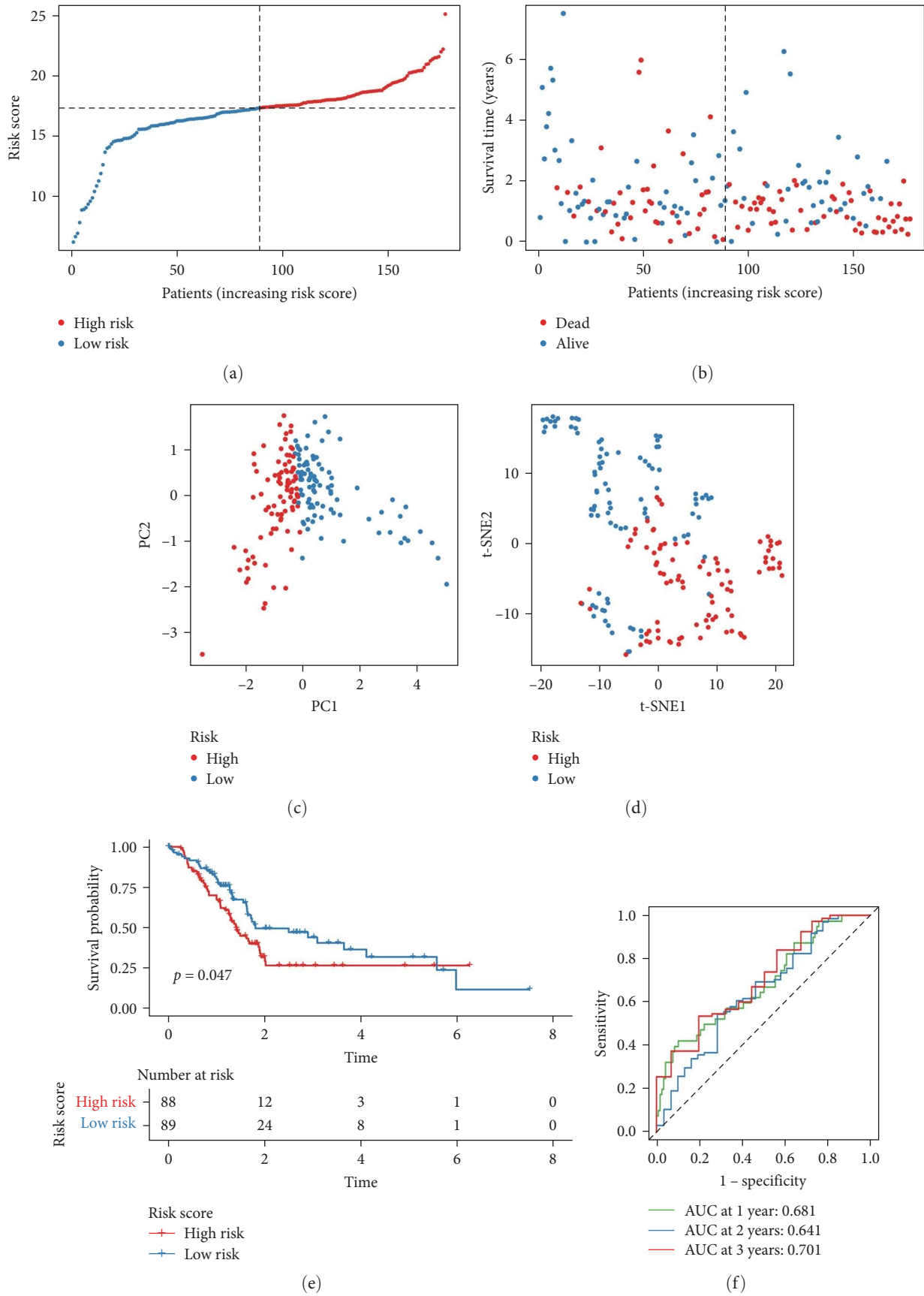
(a)

(b)

(c)

(d)

(e)

(f)

FIGURE 4: Prognostic assessment of the risk signature in the TCGA cohort: (a, b) the distribution of risk scores (a) and survival statuses (b) in the high-risk and low-risk categories; (c, d) PCA (c) and t-SNE (d) plots for PC based on the risk score; (e) Kaplan–Meier curves of overall survival in two risk groups; (f) overall survival ROC curves at 1, 3, and 5 years. PCA, principal component analysis; t-SNE, t-distributed stochastic neighbor embedding; PC, pancreatic cancer; ROC, receiver operating characteristic.
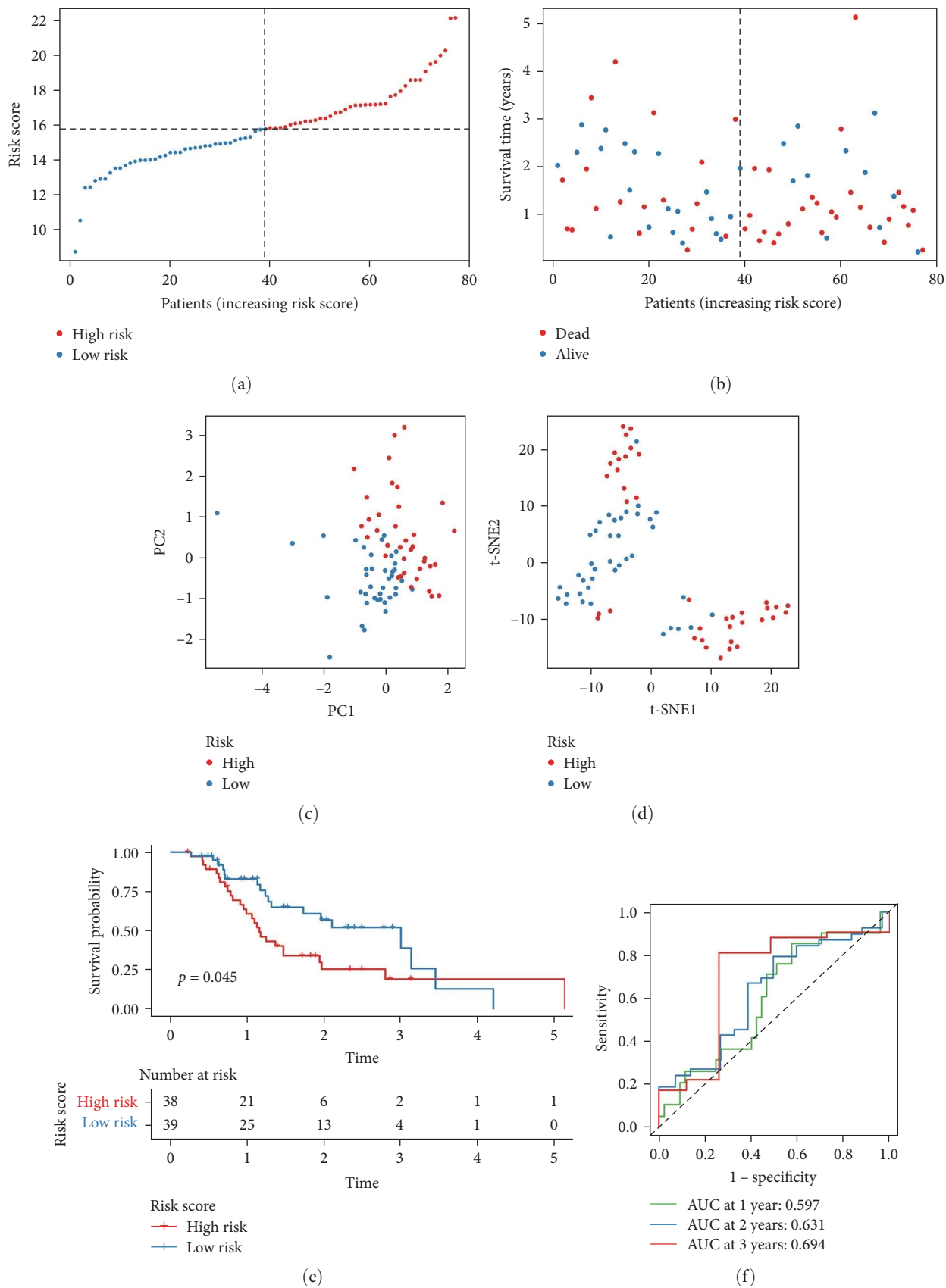
FIGURE 5: Validation of the risk signature in the ICGC cohort: (a, b) the distribution of the high-risk and low-risk groups regarding risk scores (a) and survival statuses (b); (c, d) PCA (c) and t-SNE (d) plot of the survival models; (e) Kaplan–Meier curves of overall survival for two risk categories; (f) overall survival ROC curves at 1, 3, and 5 years.
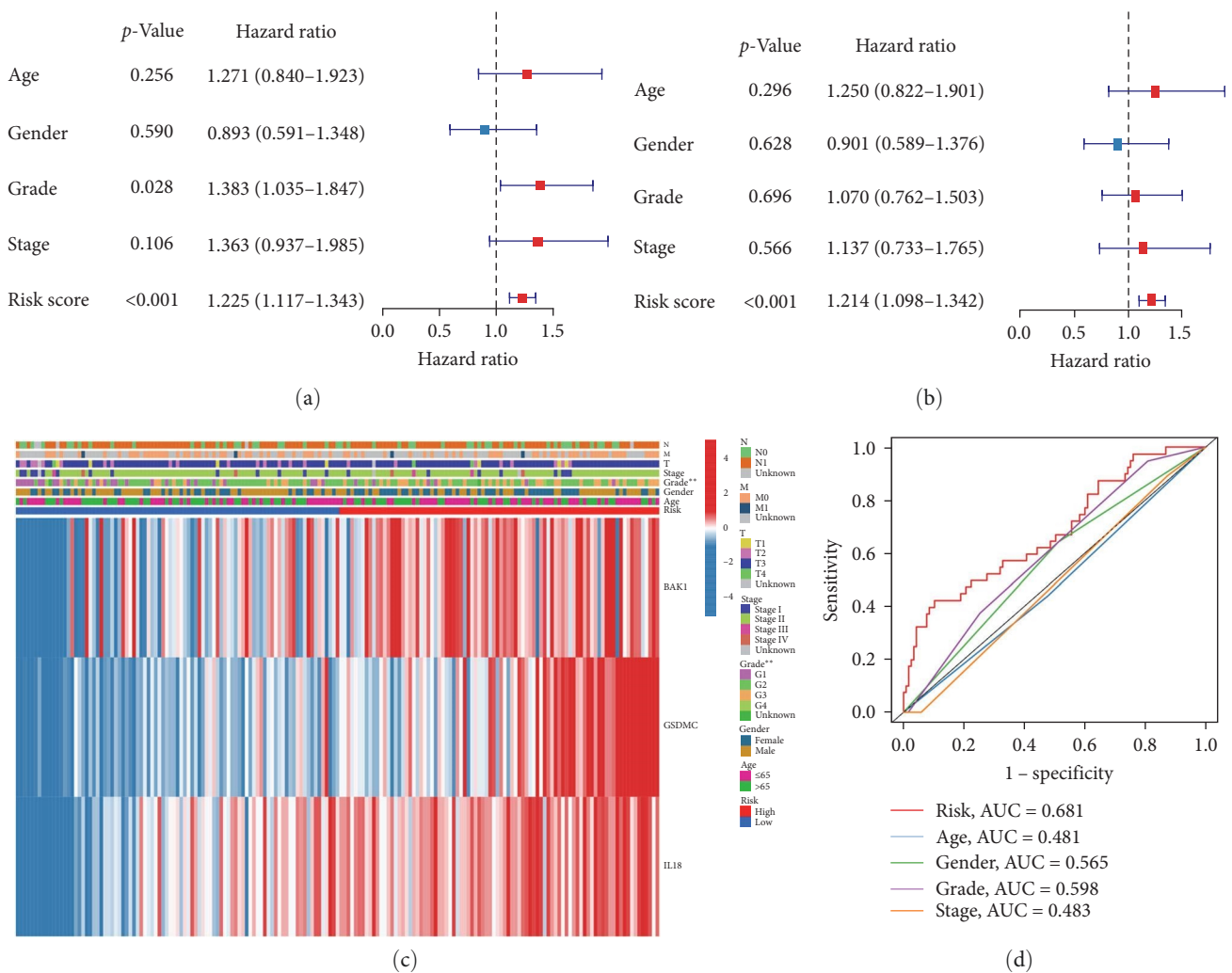
(a)

(b)

(c)

(d)

FIGURE 6: Evaluation of the independent predictive capacity of the risk score and clinicopathological characteristics in the TCGA cohort: (a, b) forest plots of univariate (a) and multivariate (b) cox regression analyses of clinicopathological characteristics and risk score; (c) heatmap of the relationships between the expression levels of three key PRGs and clinicopathological characteristics ($^*p<0.05$, $^{**}p<0.01$, $^{***}p<0.001$); (d) the 1-year ROC curves and AUC values of the risk signature and clinicopathological characteristics. AUC, area under the curve.

and subsequently compared between the two risk groups. High-risk individuals scored significantly higher in antigen-presenting cells (APCs) coinhibition, costimulation of APCs, Type I IFN responses, parainflammation, major histocompatibility complex (MHC) Class I and cGAS-STING pathway activation as compared to low-risk individuals (Figure 8(b)). The expression differences of immune checkpoints, crucial to immunotherapy, were compared in different groups. Compared with low-risk patients, the expression levels of TNFRSF14, TNFSF4, CD276, CD80, LGALS9, HHLA2, CD70, TNFSF9, TNFRSF25, TNFRSF4, CD40, TNFRSF18, TNFSF15, CD274, CD44, and TNFRSF9 in high-risk patients were significantly increased ($p<0.05$) (Figure 8(c)). Immune subtype analysis identified 56 patients with C1, 32 patients with C2, 40 patients with C3, one patient with C4, none with C5, and 21 patients with C6. Patients with C1, C2, C3, and C6 immune subtypes were included to be studied due to the absence of C5 patients and the extremely small number of C4 patients. A significant relation was discovered

between the high-risk scores and C1 (wound healing), whereas the low-risk scores were positively linked with C3 (inflammatory) (Figure 8(d)).

3.7. Somatic Mutation and m6A-Related Modification Analyses.

The 20 most frequently mutated genes in the two risk categories were depicted using waterfall plots based on somatic mutation analysis (Figures 9(a) and 9(b)). Although somatic mutation counts were not substantially different in the two risk groups ($p = 0.21$) (Figure 9(c)), high-risk patients exhibited greater levels of KRAS and TP53 mutations than low-risk patients (Figures 9(d) and 9(e)). As a result, we examined the link between KRAS mutations and TP53 mutations in both high- and low-risk groups and observed a significant correlation (Figures 9(f) and 9(g)). Mutations in KRAS and TP53 were positively associated with the expressions of BAK1, GSDMC, IL18, and KRAS but not with PD-L1 or TP53 (Figures 9(h) and 9(i)). Besides, both
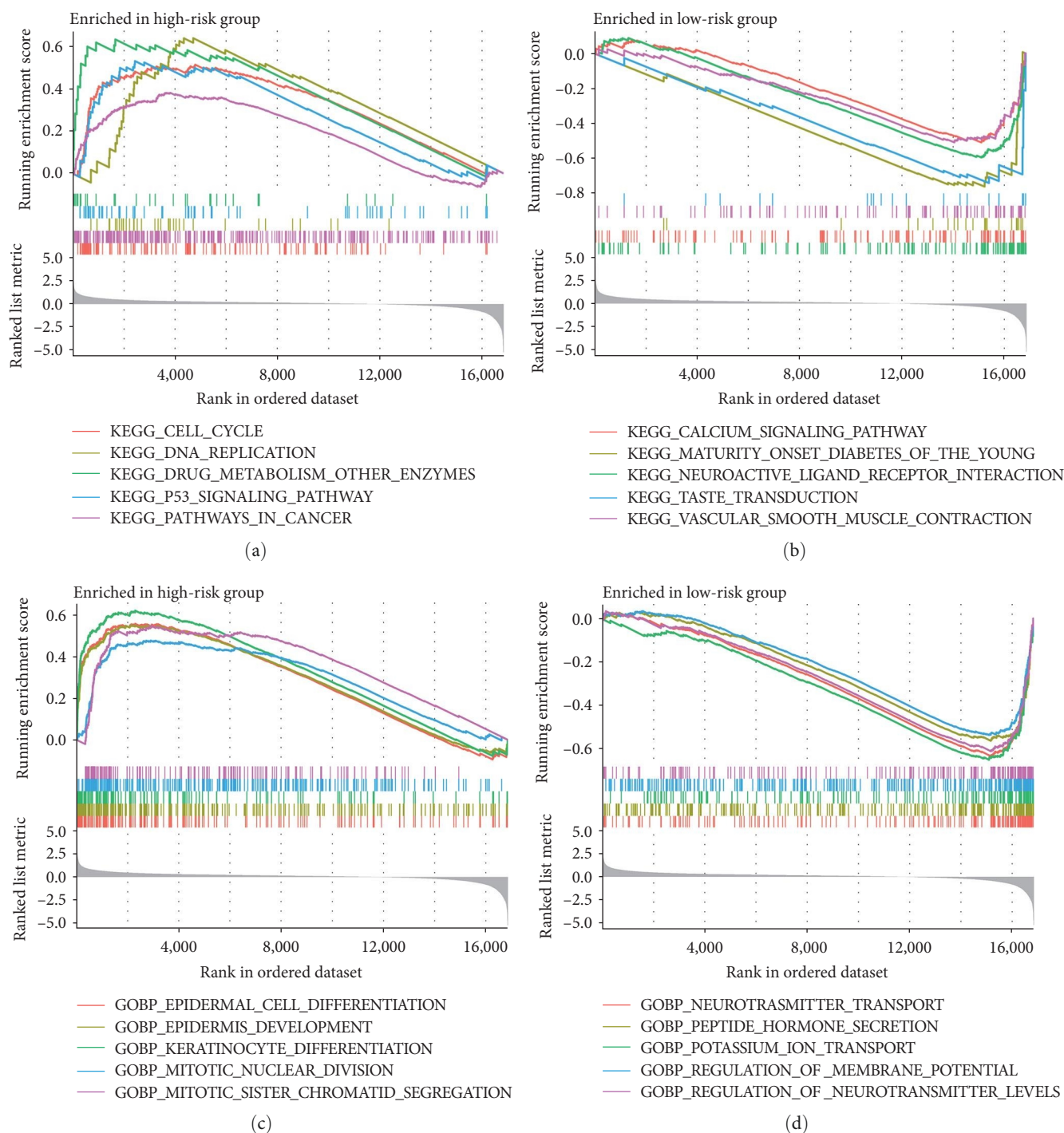
FIGURE 7: Gene set enrichment analysis (GSEA) of biological functions and pathways according to the risk signature for the TCGA cohort: (a, b) the top 5 KEGG pathways enriched in the groups with high risk (a) and low risk (b); (c, d) the top 5 GO terms enriched in the groups with high risk (c) and low risk (d). KEGG, Kyoto Encyclopedia of Genes and Genomes; GO, gene ontology.

KRAS mutations and TP53 mutations were positively related to the ssGSEA scores of hypoxia, the TNF signaling pathway, and the cGAS-STING pathway (Figures 9(j) and 9(k)). Patients with KRAS mutations had higher ssGSEA scores for the NF-kappaB pathway than those with wild-type KRAS, whereas patients with TP53 mutations had higher ssGSEA scores for MHC Class I, Type I IFN response,

parainflammation, and pyroptosis than those with wild-type TP53 (Figures 9(j) and 9(k)). The results suggest that KRAS and TP53 mutations may dominate different inflammatory pathways. We also discovered that these two mutations had different prognostic effects between PC patients at high and low risk. High-risk patients with KRAS mutations suffered an inferior outcome than those with wild-type KRAS ($p = 0.016$)
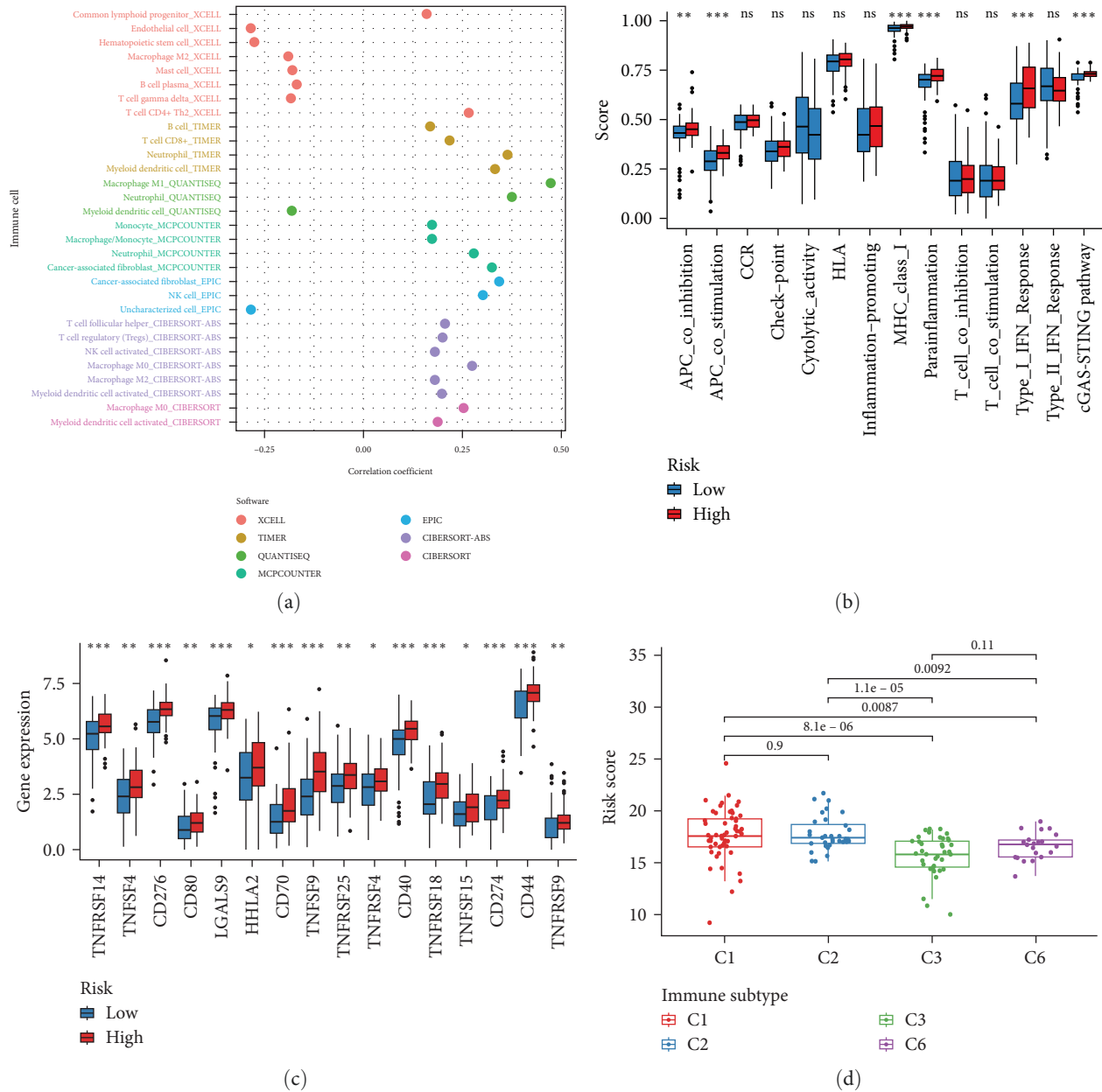
(a)

(b)

(c)

(d)

Figure 8: Comparing the immune profile of the two risk groups in the TCGA cohort: (a) association analysis of immune cell infiltration and risk scores; (b) the ssGSEA scores of 14 immune-related functions between two risk groups ($^*p < 0.05$, $^{**}p < 0.01$, $^{***}p < 0.001$); (c) different expressions of immune checkpoints between two risk groups; (d) the link of risk scores with immune subtypes.

(Figures 9(l) and 9(m)), whereas low-risk patients with mutant TP53 experienced a more adverse outcome than those with wild-type TP53 ($p = 0.009$) (Figures 9(n) and 9(o)). In addition, the two risk groups were compared for gene expression levels of m6A RNA methylation regulators, and the high-risk groups exhibited significantly greater expression of HNRNPC, RBM15, YTHDF1, and YTHDF2 (Figure 9(p)).

3.8. Drug Sensitivities. The IC$_{50}$ of three commonly used anti-cancer medications (gemcitabine, cisplatin, and erlotinib) in PC patients was estimated using the pRRophetic algorithm.

IC$_{50}$ denotes the concentration of an inhibitor needed to inhibit a biological or biochemical process by half. The high-risk group possessed significantly lower IC$_{50}$ values than the low-risk group (Figure 10(a)–10(c)), indicating that high-risk patients are more sensitive to these drugs. Spearman correlation analysis was employed to evaluate the connection between individual prognostic genes and drug sensitivity in NCI-60 cell lines from the CellMiner database. Statistical significant relationships ($p < 0.05$) were selected and ranked according to their p-values. The top 16 results are presented in *Supplementary 3*. A negative relationship was observed between the expression of GSDMC and the drug sensitivity of cancer cells to lxazomib
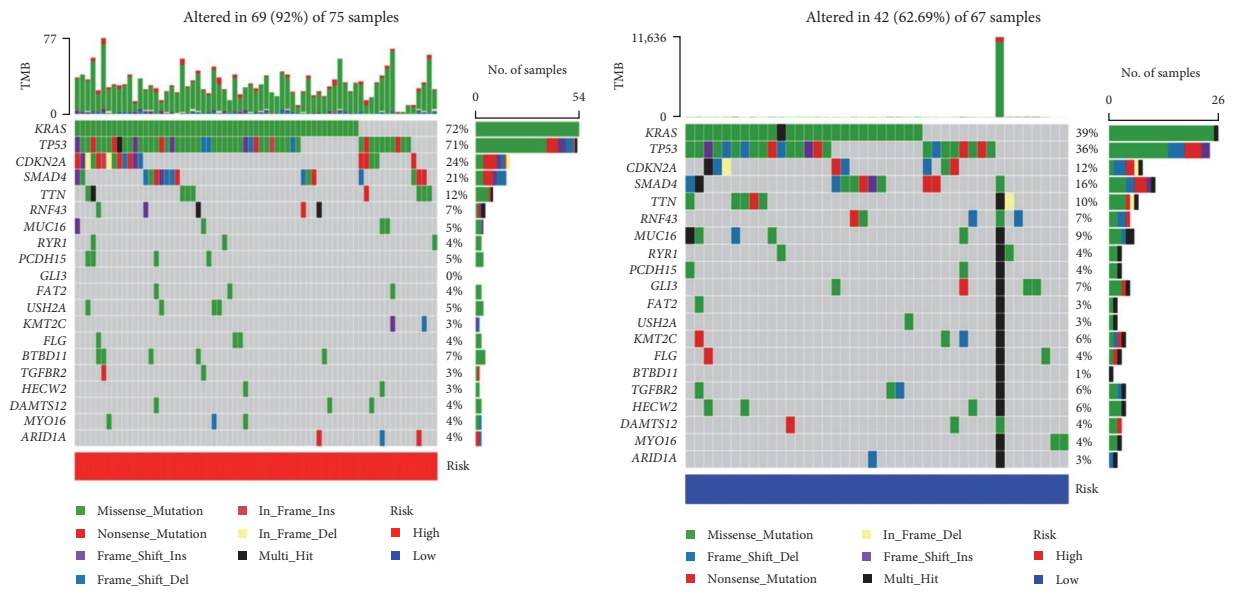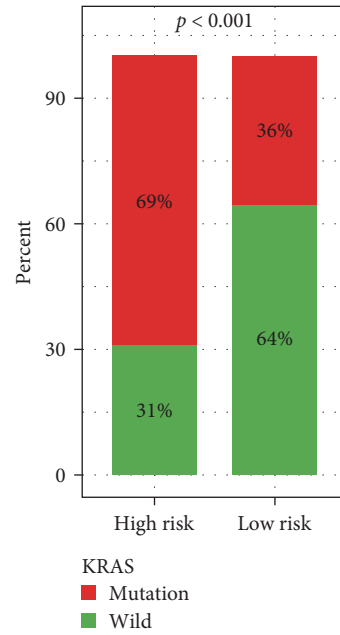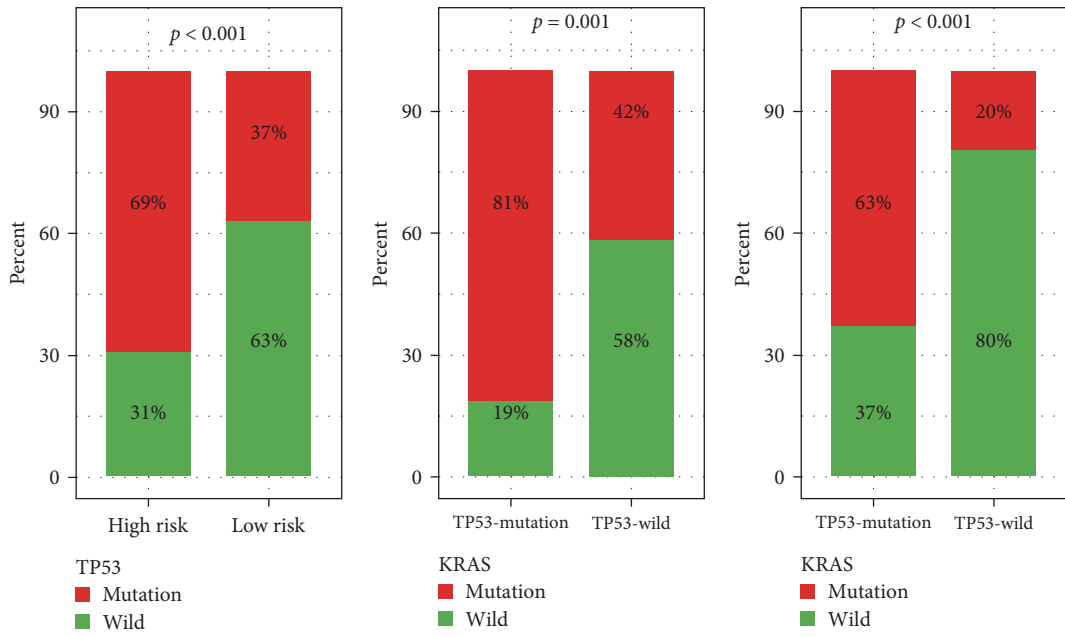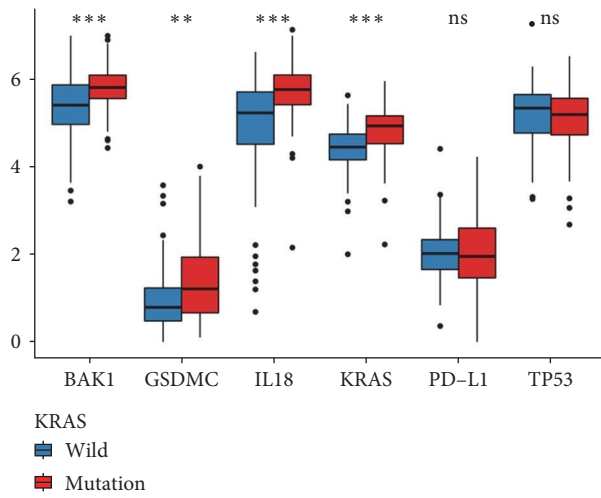
(a)

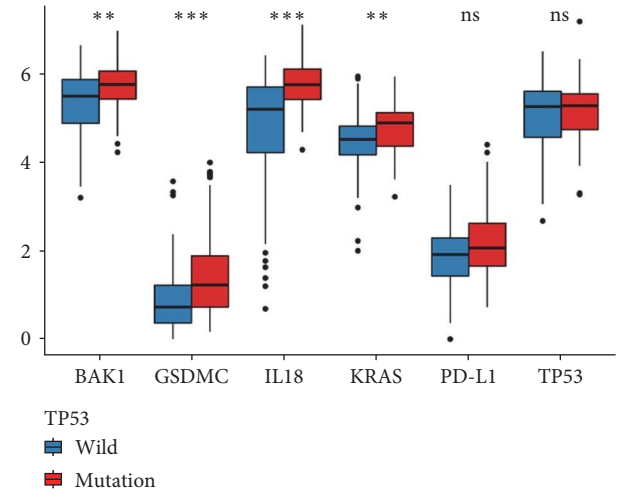
(b)
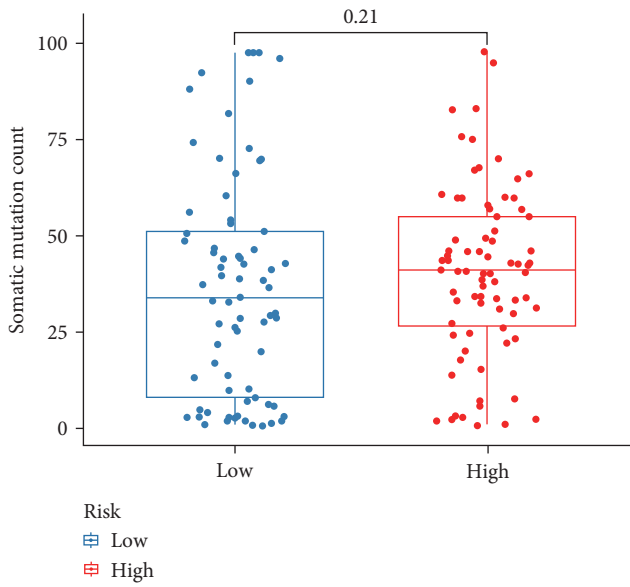
(c)

(d)

FIGURE 9: Continued.

(e)

(f)
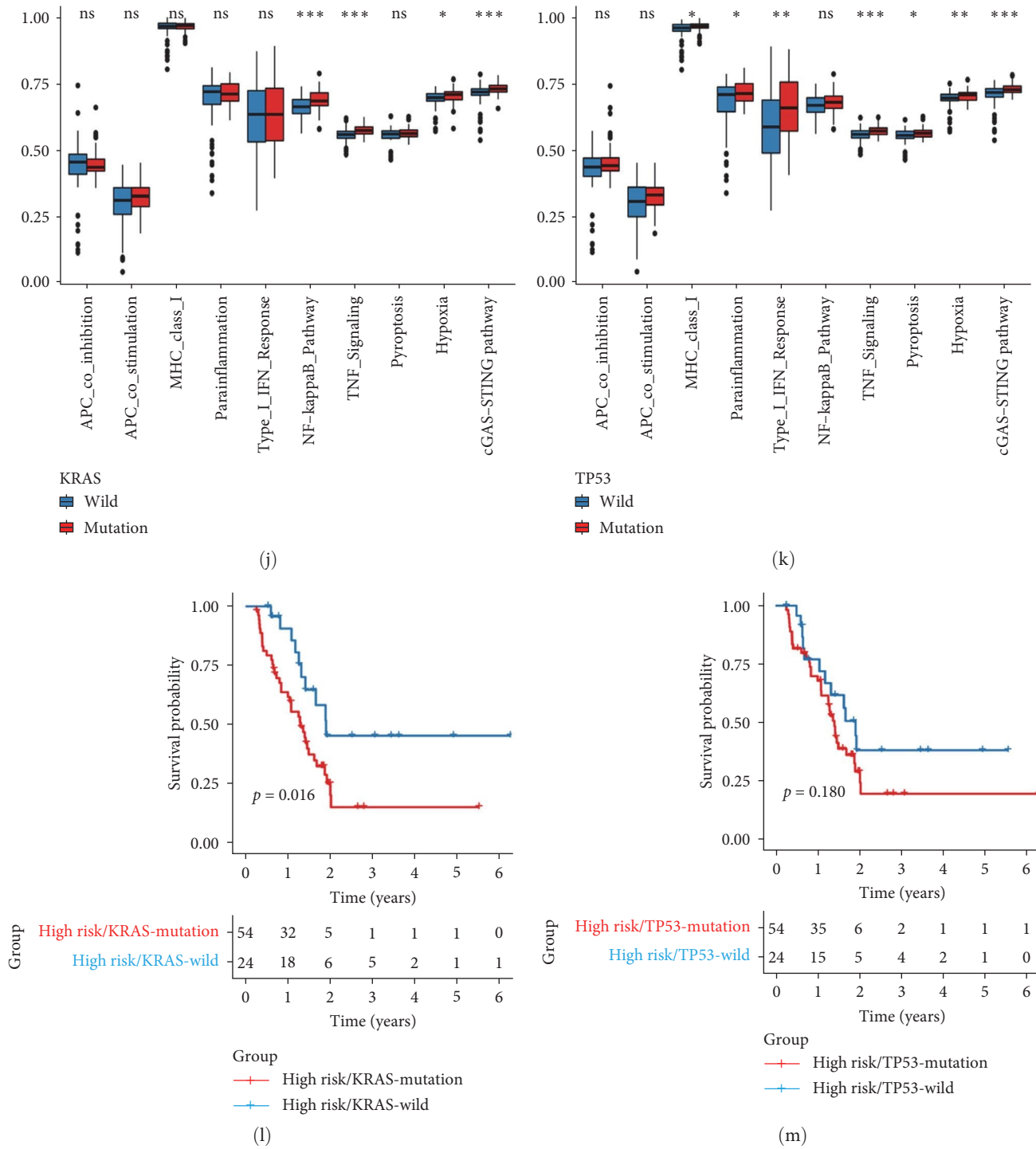
(g)

(h)

(i)

(j)

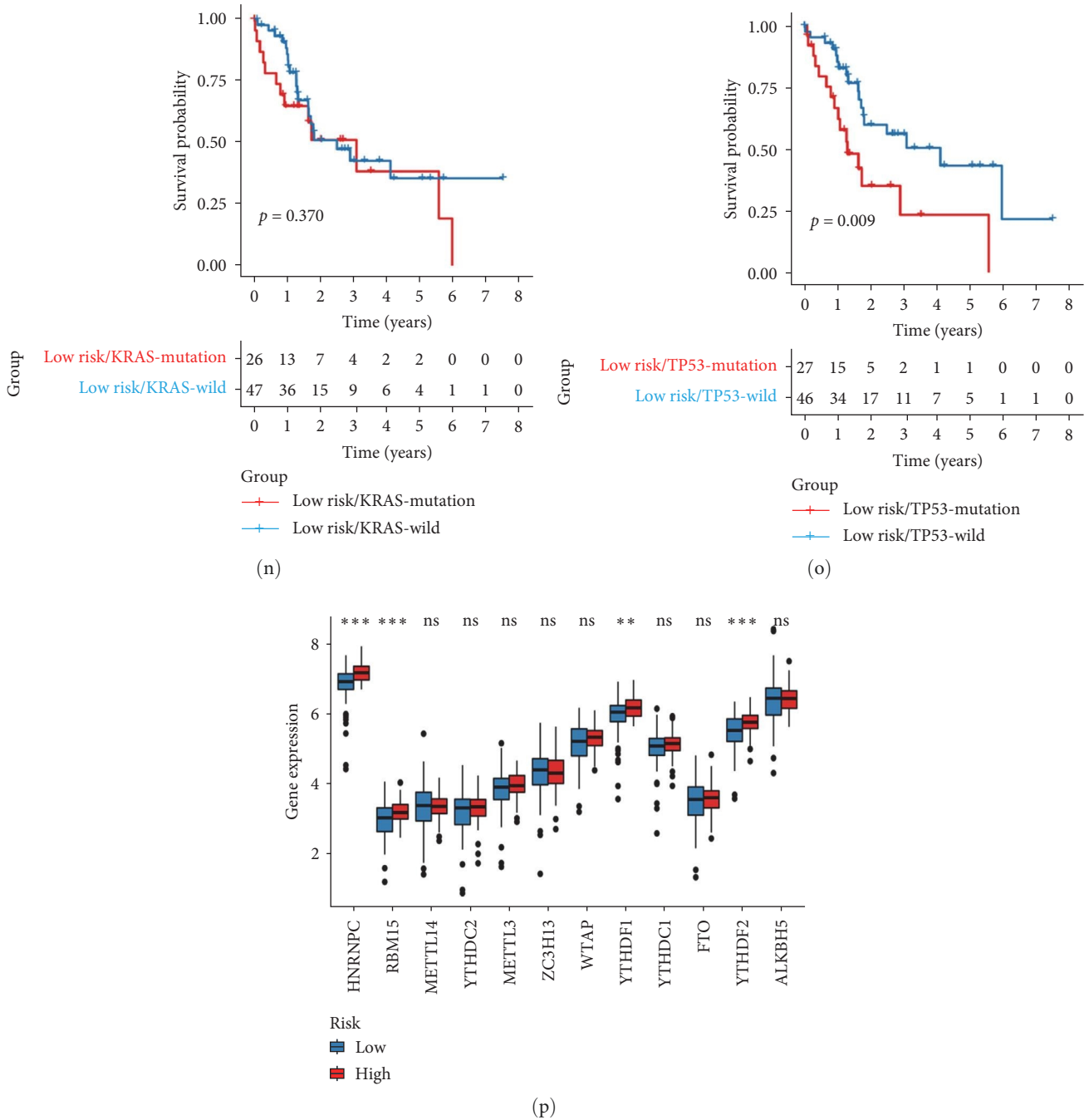(k)

(l)

(m)

FIGURE 9: Continued.

(n)

(o)

(p)

FIGURE 9: Somatic mutation and m6A-related modification between the high-risk and low-risk groups in the TCGA cohort: (a, b) waterfall plots of the top 20 genes with the highest mutation frequency in the high-risk (a) and low-risk (b) groups; (c) boxplot of somatic mutation count in the high-risk and low-risk groups; (d, e) barplots of KRAS mutations (d) and TP53 mutations (e) between the high-risk and low-risk groups; (f, g) barplots of the association of KRAS mutations with TP53 mutations in the high-risk (f) and low-risk (g) groups; (h, i) boxplots of the effects of KRAS mutations (h) and TP53 mutations (i) on expressions of 6 specific genes ($*p < 0.05$, $**p < 0.01$, $***p < 0.001$); (j, k) boxplots of the impacts of KRAS mutations (j) and TP53 mutations (k) on the ssGSEA scores of 6 immune-related functions, NF-kappaB pathway, TNF signaling pathway, pyroptosis and hypoxia; (l, m) Kaplan–Meier survival curves of KRAS mutations (l) and TP53 mutations (m) in the high-risk group; (n, o) Kaplan–Meier survival curves of KRAS mutations (n) and TP53 mutations (o) in the low-risk group; (p) comparison of gene expression of m6A RNA methylation regulators for the two risk groups.

citrate, midostaurin, bortezomib, and pralatrexate. Similarly, upregulated IL18 expression increased cancer cell resistance to some drugs, such as pipamperone, bortezomib, actinomycin, and so on.

3.9. TMB, MSI, and Immunotherapy. The risk signature and TMB underwent a correlation analysis. High-TMB was defined as more than 20 muts/Mb, intermediate-TMB as 6–19 muts/Mb, and low-TMB as fewer than 5 muts/Mb [56]. Almost all patients
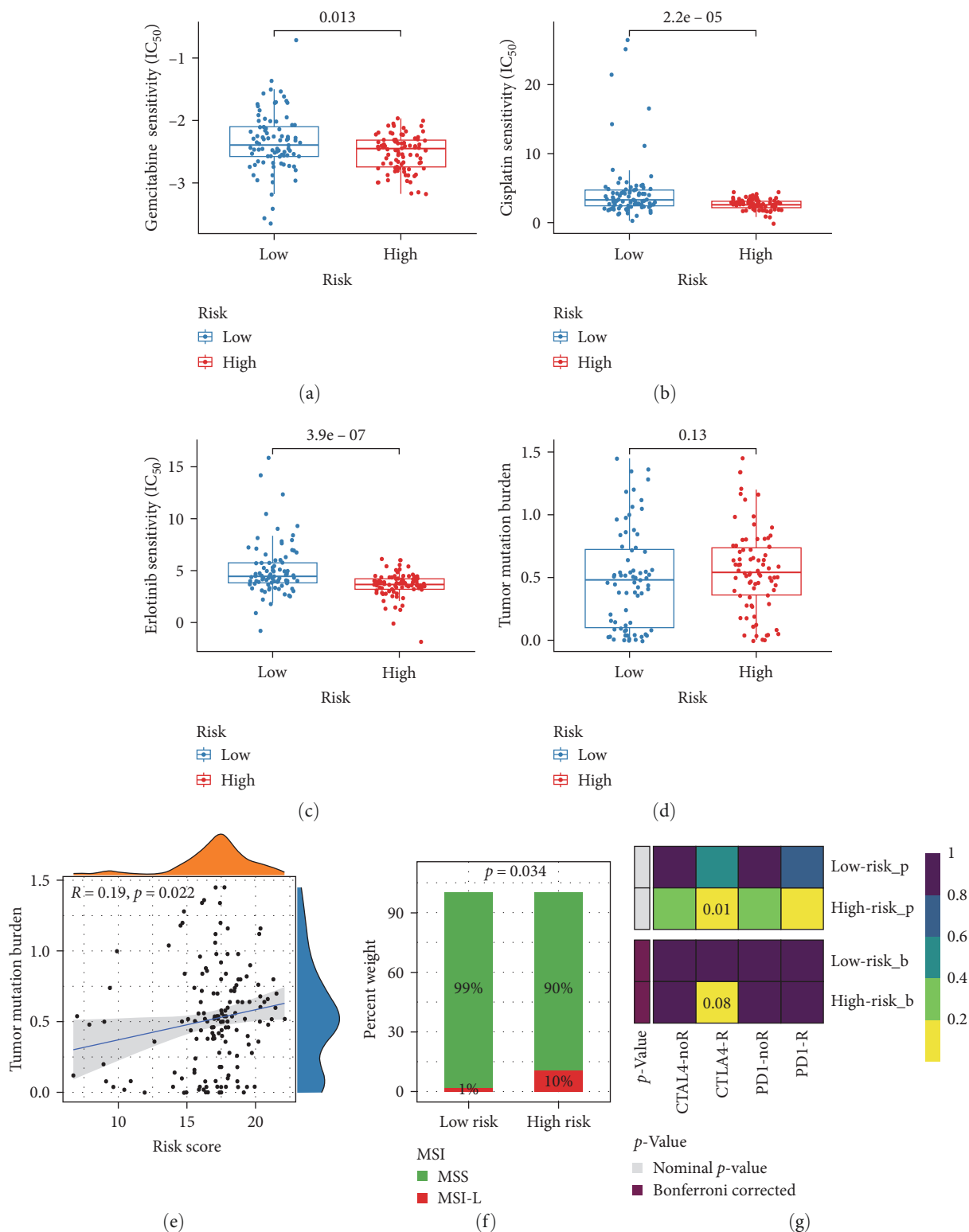
FIGURE 10: Correlation of the risk signature with drug sensitivity, TMB, MSI, and immunotherapy in the TCGA cohort: (a–c) assessment of sensitivity to gemcitabine (a) cisplatin (b), and erlotinib (c) in two risk groups; (d) boxplot of TMB in the high-risk and low-risk groups; (e) Spearman correlation of risk scores with TMB; (f) comparing the proportion of MSI in two risk groups; (g) subclass mapping analysis to predict ICIs treatment response in different risk groups. MSS, microsatellite stability; MSI-L, low microsatellite instability; ICIs, immune checkpoint inhibitors.

had a low-TMB (median = 0.52 muts/Mb, range: 0–1.45 muts/ Mb), except for one patient with a high-TMB (238.38 muts/Mb). The TMB did not differ significantly between the low- and high-risk categories ($p = 0.13$, Figure 10(d)), but the Spearman correlation analysis revealed a positive relationship of the risk scores with the TMB ($R = 0.19$, $p = 0.022$, Figure 10(e)). Also, MSI was estimated for the two risk groups. There were 140 patients with microsatellite stability (MSS), nine patients with low MSI (MSI-L), and none with high MSI (MSI-H). In comparison to the low-risk group, the high-risk group had a higher prevalence of MSI-L (Figure 10(f)). Subclass mapping analysis was then applied to predict the response of different risk groups to ICIs therapy. The result manifested that the high-risk group had a greater chance of responding to anti-CTLA-4 therapy ($p = 0.01$), but Bonferroni adjusted p-value was 0.08 (Figure 10(g)).

4. Discussion

The discovery of novel and effective molecular targets is crucial for diagnosing and treating PC due to its dismal prognosis and the limited traditional diagnostic and therapeutic strategies. The field of PCD has gained much attention in tumor biology research. Pyroptosis, an inflammatory form of PCD, has been demonstrated to participate in the progression of cancer, immunotherapies, and chemotherapies [57, 58]. However, pyroptosis in PC has not been fully elucidated in terms of its mechanisms and functions. Thus, we developed a pyroptosis-associated gene signature to explore its significance in PC patient prognosis, TIME, and treatment.

We obtained 57 genes associated with pyroptosis based on a previous study and the MSigDB. Because of the insufficient samples of the normal pancreas in the TCGA dataset, 26 PRGs with differential expression between PC and normal tissues were found in the TCGA TARGET GTEx dataset via three approaches. Twenty-four PRGs were enrolled in the TCGA cohort for further analysis, except for two genes without expression data. Ten PRGs were substantially associated with the prognosis of PC patients, as determined by univariate Cox regression. Our next step was to perform LASSO Cox regression and random forest analyses, and three PRGs (BAK1, GSDMC, and IL18) were selected as signature genes to construct a risk model. These three genes were more highly expressed at the mRNA level in PC tissues compared to normal pancreatic tissues, and their expressions were significantly associated with poor outcomes. IHC analysis from the HPA database confirmed that PC tissues overexpressed BAK1 and IL18 proteins compared to normal tissues, whereas neither PC tissues nor normal tissues had any detectable GSDMC protein. PC patients were divided into two categories, high- and low-risk, based on their median risk scores. Patients at higher risk had a worse outcome than those at lower risk. Both the univariate and multivariate Cox regression analysis revealed a significant relationship between the risk model and OS. The risk signature's accuracy in predicting prognosis was confirmed by time-dependent ROC curves, which also showed that it was a more reliable prognostic predictor than clinicopathological characteristics in PC patients. More importantly, the risk model was verified

to be robust and exhibited well-predictive capability in the ICGC cohort.

The BAK1 gene encodes the BAK protein. BAK, belonging to the BCL2 protein family, is a proapoptotic effector protein. Upon activation, BAK or BAX permeabilizes the outer membrane of mitochondria, allowing apoptogenic substances into the cytosol (such as cytochrome c) and activating caspase [59–61]. Activation of BAX and BAK by chemotherapeutic agents can initiate the sequential activation of caspase-9 and caspase-3. The latter facilitates GSDME cleavage to produce N-termini, resulting in pyroptosis [57, 62]. Based on immunohistochemistry tests performed by Evans et al. [63] in PDAC and ampullary cancer, BAK expression was higher in malignant epithelia compared to acini and major ducts but lower in malignant epithelia compared to minor ducts. However, Graber [64] noted that although BAK mRNA expression in pancreatic tumor samples was 2.5-fold higher than that in the normal samples, elevated BAK expression in PC occurred in peritumoral tissue with chronic inflammation rather than in the tumor cells themselves.

GSDMC, a pore-forming protein's precursor, is cleaved to liberate its N-terminal moiety, which induces membrane permeabilization and results in cell pyroptosis. Previous research has demonstrated that GSDMC acts as an oncogene to facilitate the proliferation and metastasis of tumor cells [65, 66]. In this study, GSDMC protein level was not detected in PC tissues or normal pancreatic tissues according to the results of the HPA database, which might be due to the low sensitivity of the selected IHC antibody. Xia et al. [67] verified by IHC staining analysis that elevated GSDMC expression is linked with a shorter OS in PDAC. Hou et al. [68] found that p-Stat3 increased PD-L1 nuclear translocation in hypoxic conditions, and these two factors combined boosted GSDMC transcription. Following TNF-alpha treatment, GSDMC is cleaved by activated caspase-8, causing tumor necrosis and pyroptosis. Notably, chronic tumor necrosis facilitates tumor growth and metastasis [69] and restrains antitumor immunity [68]. In addition, a poor prognosis was also discovered to be associated with increased GSDMC expression in breast cancer [68], lung adenocarcinoma [70], and kidney clear cell cancer [71].

IL18, as a pro-inflammatory cytokine, is constitutively expressed in monocytes, DCs, macrophages, and epithelial cells [72, 73]. The cytokine regulates innate and adaptive immune responses by influencing monocytes, DCs, NK cells, T cells, and B cells [74]. IL18 exhibits dual functions in regulating tumor cells and tumor microenvironment (TME). On the one hand, IL18 shows anticancer effects by facilitating the proliferation of NK cells and T lymphocytes [74]. On the other hand, IL18 participates in tumorigenesis and progression. It leads to tumor metastasis by proangiogenic action [75] and promotes the invasiveness of carcinoma cells by causing matrix metalloproteinase-9 (MMP-9) production [76]. Zhao et al. [77] discovered that IL18 derived from PDAC cells activates the PD-1/PD-L1 pathway by binding to its receptor on the surface of regulatory B cells, contributing to immune tolerance. In addition, IL18 enhances PC-cell proliferation and invasion via the NF-kappaB pathway [78]. The elevated

level of IL18 induces Th1 immune responses characterized by hypersecretion of IFN-gamma and TNF-alpha, which are engaged in chronic inflammation [79]. A positive connection has been demonstrated between PC onset and chronic inflammation [80]. Chronic inflammation can generate conditions that promote malignant transformation by the gradual amassment of gene mutations and contribute to tumor cell proliferation and neovascularization [80]. IL18-binding protein (IL18BP), an antagonist to IL18 activity, possesses a high affinity for mature IL18 and blocks the interaction of IL18 with receptors on the cell surface [81]. Carbone et al. [79] found that the levels of free serum IL18 and IL18BP in PDAC patients were substantially higher than in healthy controls and that elevated serum levels of free IL18 were linked with an inferior outcome. This may be due to the imbalanced relationship between IL18 and IL18BP that influences the pathogenesis and progression of PC. However, one study by Guo et al. [78] observed that greater IL18 levels in PC tissues were linked with a shorter OS, whereas higher plasma IL18 levels were linked with a longer OS. In summary, IL18 overexpression might affect the development and progression of PC.

In this study, patients at high risk possessed relatively higher immune cell infiltration (including B cells, Th2 cells, CD 8+ T cells, Treg cells, Tfh cells, neutrophils, M0 macrophages, NK cells, M1 macrophages, mDCs, M2 macrophages, and CAFs) and more active immune functions or pathways (including APC costimulation, MHC Class I, parainflammation, APC coinhibition, Type I IFN response, and the cGAS-STING pathway) compared to patients at low risk. The immunosuppressive characteristics of the high-risk group verify the immune modulation ability of pyroptosis and affect PC patients' prognosis. Underlying mechanisms are unclear, but parainflammation, a low inflammatory response between homeostasis and chronic inflammation [82], may participate in tumor initiation, invasion, metastasis, pyroptosis, and the formation of an immunosuppressive microenvironment in PC.

Parainflammation is characterized by Type I IFN response and TP53 mutation and is correlated with a worse prognosis [45]. Similarly, this study revealed that the patients at high risk exhibited a higher level of parainflammation, a stronger Type I IFN response, and higher TP53 mutations compared to patients at low risk. Parainflammation is caused by internal cell insults and is tightly associated with cellular senescence [83]. However, when TP53 mutations cause loss of p53 protein function, parainflammation shifts from cancer suppression to cancer promotion [83]. Thus, parainflammatory tumors tend to exhibit a high rate of TP53 mutations. Rapidly proliferating tumor cells are often afflicted with hypoxia, nutritional deficiencies, and energy shortages due to inadequate vasculature and blood supply [84]. Apoptosis will occur in cancer cells that cannot adapt to hypoxia [85]. As proapoptotic effector proteins, BAX and BAK modulate the permeability of the external mitochondrial membrane, which causes the translocation of cytochrome c and mitochondrial DNA (mtDNA) into the cytoplasm [86]. Multiple sensors of cytosolic DNA, namely absent in melanoma 2

(AIM2), Z-DNA binding protein 1(ZBP1), and cyclic GMP-AMP synthase (cGAS), exist for triggering innate immune responses in the cell [87]. mtDNA can effectively ignite the cGAS-STING-TBK1 signaling pathway, inducing the generation of Type I IFNs through activation of IFN-regulatory factor 3 (IRF3) and the production of other pro-inflammatory cytokines, which include IL-18 and IL-1β, via activating NF-kappaB pathway [88]. Type I IFNs attach to the IFN-alpha/beta receptor (IFNAR) complex and start the JAK/STAT downstream pathway, which triggers the transcription of IFN-stimulated genes [88] such as AIM2 [89] and ZBP1 [90]. Upon recognition of cytosolic DNA, ZBP1 initiated NLRP3 inflammasome activation through the RIPK1-RIPK3-caspase-8 axis [91]. Cytosolic DNA can also activate the AIM2 inflammasome. NLRP3 and AIM2 inflammasomes both initiate caspase 1, stimulating pro-IL-1 and pro-IL18 maturation. Under hypoxia, the PD-L1/p-Stat3 complex enhances GSDMC expression, which is subsequently cleaved with activated caspase-8, resulting in pyroptosis and the liberation of IL-1β and IL18 [68]. It is suggested that GSDMC expression is relevant to PD-L1 expression and hypoxic TME. Type I IFNs can increase PD-L1 expression [92]. Parainflammation characterized by Type I IFN response was observed to have a positive relationship with PD-L1 expression in PC (Figure 11). Hypoxia enhances tumor invasiveness, metastasis, and angiogenesis [93]. Of note, the risk score was positively related to NF-kappaB-mediated inflammatory response in the study. However, the ssGSEA score of pyroptosis did not correlate with the ssGSEA score of the NF-kappaB pathway; instead, it correlated significantly with the ssGSEA scores of Type I IFN response. In summary, the parainflammatory response in PC may be involved in GSDMC-induced pyroptosis through cytosolic DNA-sensing pathways under hypoxic conditions. The Spearman correlation heatmap (Figure 11) shows the relationship discussed above.

According to the somatic mutation analysis, patients at high risk presented a greater frequency of KRAS and TP53 mutations than patients at low risk. KRAS and TP53 mutations were positively correlated with the expressions of BAK1, GSDMC, IL18, and KRAS. Intriguingly, although KRAS mutations were significantly associated with TP53 mutations in two risk groups, these two gene mutations were involved in different inflammatory pathways and played different prognostic roles in distinct risk categories. Patients with KRAS mutations in the high-risk category possessed higher ssGSEA scores of the NF-kappaB pathway and a less favorable outcome than those with wild-type KRAS, while patients with TP53 mutations in the low-risk category possessed higher ssGSEA scores of parainflammation, Type I IFN response and pyroptosis and an unfavorable prognosis than those with wild-type TP53. The results also demonstrated that TP53 mutations rather than KRAS mutations played a significant part in parainflammatory response and pyroptosis in PC.

PC is characterized by desmoplasia and an inflammatory environment [94]. Cytokines participate in the interaction between immune cells and tumor cells [95]. IFNs encompass a broad family of cytokines that act as pivotal promoters of
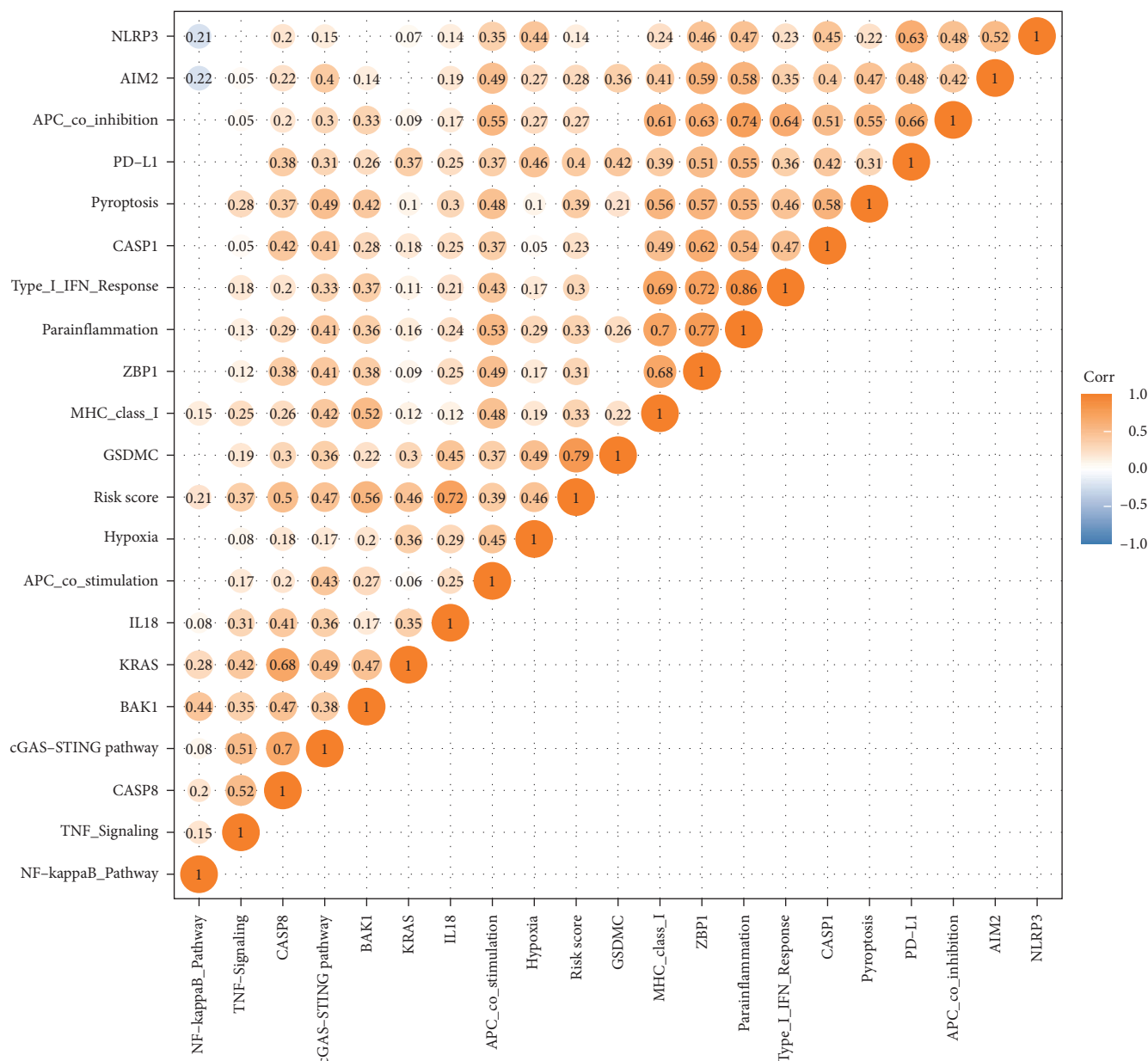
FIGURE 11: Spearman correlation heatmap of the risk score, expressions of 10 critical genes, and the ssGSEA scores of 10 gene sets (6 immune-related functions, NF-kappaB pathway, TNF signaling pathway, pyroptosis, and hypoxia).

inflammation in the TME [96]. Type I IFNs are crucial for the TME of PC because they operate on immune and tumor cells, respectively, to prevent tumor development directly and indirectly [97]. They boost antitumor immunity by stimulating CD4+ helper T cells, CD8+ cytotoxic T cells, NK cells, DCs, and M1 macrophages while inhibiting Treg cells, myeloid-derived suppressor cells (MDSCs), and M2 macrophages [88]. Moreover, Type I IFNs activate DCs and enhance CD8+ T cell cross-priming. DCs, especially myeloid/conventional DC1 (cDC1), have a strong potential for processing antigens derived from tumor cells and cross-presenting these antigens through MHC class I to activate CD8+ T cells [98, 99]. However, chronic activation of the Type I IFN pathway or prolonged Type I IFN signaling may evoke immune suppressive mechanisms in cancer [100] and cause resistance to different cancer treatments [95], including ICIs resistance [101]. In the advanced phase of cancer progression, persistent Type I IFNs can upregulate indoleamine 2,3-dioxygenase and PD-L1 expressions on DCs and other myeloid cells, suppressing antitumor immunity [102]. This study also revealed a significantly positive connection between ssGSEA scores of Type I IFN response and PD-L1 expression (Figure 11). Therefore, parainflammation related to Type I IFN response may facilitate an immunosuppressive microenvironment in PC. NSAIDs have the potential to be of particular benefit to these PC patients with parainflammatory features, since NSAIDs attenuate human parainflammation.

MDSCs are a subset of bone marrow cells that express CD11b and Gr1 and are involved in immunosuppression [103]. The cells are typically categorized into two major cell subpopulations: monocytic (M)-MDSCs and granulocytic or polymorphonuclear (G/PMN)-MDSCs [104, 105]. Neutrophils resemble (G/PMN)-MDSCs in both phenotype and morphologyare. Neutrophils were a critical cell type in the TME of patients at high risk. It might be because PC cells attract neutrophils to the TME, inhibiting the immune response and promoting tumor progression. Neutrophils induce angiogenesis via MMP-9 [106] and promote epithelial-to-mesenchymal transition via elastase [107] in PDAC. Clinically, a high ratio of neutrophils to lymphocytes correlates positively with a poor prognosis in PDAC [108, 109]. Treg cells, known as antitumor immunosuppressants, can downregulate the activities of NK cells and T cells (CD4+ and CD8+). Transforming growth factor-beta and IL-10 produced by Treg cells have been demonstrated to suppress immune responses [110]. An elevated abundance of tumor-infiltrating Treg cells impairs the antitumor activity of CD8+ T cells and portends a worse prognosis in PDAC [111]. High-risk individuals also owned a greater abundance of T2 cells compared to low-risk individuals in this study. Increased Th2/Th1 ratio within the tumor-infiltrating cells indicated an inferior prognosis for PC patients with stage IIB/III [112]. The two main categories of tumor-related macrophages are "M1" and "M2" macrophages. M1 macrophages release pro-inflammatory cytokines that inhibit tumor growth, while M2 macrophages release anti-inflammatory cytokines that may promote tumor development [113]. Hu et al. [114] verified that M2 macrophage infiltration was negatively related to PC patients' prognosis. Moreover, CAFs were crucial to the TIME of high-risk patients. CAFs are the principal cell type of the desmoplastic stroma in PC [115] and interact with tumor cells via various cellular pathways [116]. Once activated, myofibrotic CAFs or inflammatory CAFs undermine the anticancer immune response and accelerate the progression of PC [117].

Sixteen immune checkpoint molecules, which positively and negatively regulate immune responses, were overexpressed in high-risk individuals compared to high-risk individuals. It was demonstrated that high TNFSF9 expression was significantly linked with immune infiltration and poor OS in PC [118]. The research by Zhao et al. [119] revealed higher expression of B7-H3 (also called CD276) in PC patients than in normal controls, and its overexpression facilitates tumor progression. Also, increased expression of B7-H3 promotes cancer progression in primary hepatocellular carcinoma [120] and predicts a shorter OS in colorectal carcinoma [121]. PD-L1 (CD274) belongs to the B7 family [122] and is expressed on the cancerous cell membranes of various solid malignancies [123], including PC [124]. The interaction of PD-L1 with PD-1 protects cancerous cells from T-cell attack and contributes to their exhaustion [125]. Several studies have reached the same conclusion that increased PD-L1 expression in tumor tissues is implicated in the adverse prognosis of PC [124, 126, 127]. The function of other immune checkpoint molecules in PC has rarely been reported and requires further investigation.

An analysis of the relationship between risk scores and immune subtypes found that high-risk scores were strongly linked with C1 (wound healing), whereas low-risk scores were significantly linked with C3 (inflammatory). Thorsson et al. [49] identified 6 immuno-subtypes across carcinoma types and described their different features. C1 (wound healing) exhibited upregulation of angiogenic gene expressions, high KRAS and TP53 mutations, elevated proliferation rate, and high infiltration of Th2 cells [49]. Similarly, this study demonstrated that high-risk individuals had high frequencies of KRAS and TP53 mutations and increased Th2 cell infiltration in cancerous tissues. Oncogenic KRAS mutations have been confirmed to participate in fibro-inflammatory microenvironment development, tumorigenesis, and growth in PC [94, 128]. Wormann et al. [129] discovered that TP53 mutation or absence of p53 function in pancreatic tumors of mice activates the JAK2-STAT3 signaling pathway, which reduces fibrosis and the abundance of stellate cells in the stroma of pancreatic tumors and alters the types of immunocyte infiltration, promoting tumor growth, and stroma modification. C3 (inflammatory) had the most prominent Th17 signature, low to moderate neoplastic cell multiplication, increased Th1 genes, and decreased overall somatic copy number [49]. In addition, C3 had a better prognosis than other subtypes (including C1), which might be because C3 had a balanced immune response [49].

The m6A modification affects many malignancies by either increasing the expression of oncogenes or decreasing the expression of carcinoma suppressor genes [130, 131]. HNRNPC, RBM15, YTHDF1, and YTHDF2 expression levels were significantly higher in the current study's high-risk individuals than in the low-risk individuals. Huang et al. [132] concluded that elevated expression of HNRNPC promotes tumor spread, rendering PDAC patients with a dismal prognosis. In hepatocellular carcinoma [133] and laryngeal squamous cell carcinoma [134], overexpression of RBM15 was reported to accelerate tumor growth and indicate a poor prognosis. YTHDF1 was discovered to boost antigen decomposition in the phagosome and prevent DCs from cross-presenting neoantigens, hence suppressing antitumor immunity [135, 136]. High YTHDF1 expression is related to an adverse prognosis in ovarian cancer [137] and breast cancer [138]. One research by Guo et al. [139] revealed that YTHDF2 is implicated in PC progression by cooperating with ALKBH5, an RNA demethylase.

The results of our estimation of the connection between these three gene expressions and medication sensitivity showed that GSDMC and IL18 expressions were adversely associated with the sensitivity of the medications presented in this study. Antitumor drugs such as gemcitabine, cisplatin, and erlotinib are generally recommended for PC treatment. As a result, we investigated the sensitivity of PC to these medications and discovered that high-risk tumors were more responsive to the medicines compared to low-risk tumors, implying that high-risk individuals may benefit from these therapies.

Moreover, ICIs therapy has exhibited impressive efficacy in the management of several solid tumors. In the present

study, subclass mapping analysis suggested that high-risk individuals owned a higher likelihood of responding to anti-CTLA-4 treatment but with a Bonferroni-corrected p-value of 0.08. Increasing evidence indicates that ICIs therapy may be beneficial for patients with high-TMB and MSI-H [140, 141]. The association of risk scores with TMB and MSI was therefore examined. The risk scores and TMB showed a positive association, and MSI-L was more common in high-risk individuals than in low-risk individuals. However, almost all patients included in the study exhibited low-TMB and no MSI-H. Mismatch repair deficiency (dMMR)/MSI-H is presently the single reliable biomarker available for predicting immunotherapy response in PC patients [142]. As this population partially overlaps with high-TMB PC, and high-TMB/MSI-H PC represents a very small population, immunotherapy currently benefits only a tiny number of PC patients. The mainstay of treatment for most PC patients remains cytotoxic chemotherapy. Combining conventional therapy with targeted therapy and immunotherapy may create a promising PC therapeutic option.

However, this research has some restrictions to be noted. First, the risk signature was the lack of prospective data validation. Second, the exact function of these three gene combinations remains undetermined and requires additional experiments to confirm. Third, the risk score's relationship with the tumor microenvironment requires to be determined experimentally. Fourth, the mechanism of parainflammation-induced pyroptosis needs to be validated in experiments.

5. Conclusions

A novel PC prognostic model with three PRGs was developed in this study. High-risk individuals possessed different molecular pathways, higher KRAS and TP53 mutations, increased expression of PD-L1, C1 immune subtype, and immunosuppressive microenvironment characterized by parainflammation compared to low-risk individuals. Besides, parainflammatatory response was crucial in PC pyroptosis. Consequently, the risk model may help discover novel biomarkers and offer fresh insights into predicting prognosis, exploring the TIME, and developing management strategies for PC patients.

Data Availability

The data supporting the findings of the present study are available upon request from the corresponding authors. All datasets in this study were downloaded from public databases.

Conflicts of Interest

The authors declare that they have no conflicts of interest.

Authors' Contributions

Kong-kong Wei and Hao Chen designed this study. Kong-kong Wei and Zhi-xing Du collected the data. Kong-kong Wei, Zhi-xing Du, and Jun-ge Deng analyzed the data and interpreted the findings. Kong-kong Wei drafted the manuscript, which was revised by Jin-wei Yang and Hao Chen. Hao Chen obtained the funding and directed the research. The manuscript has been reviewed and approved by all authors.

Supplementary Materials

Supplementary 1. 57 pyroptosis-associated genes and 47 immune checkpoint genes.

Supplementary 2. IHC analysis of the protein expression of three signature genes in the Human Protein Atlas database.

Supplementary 3. Scatter plots of the connection between drug sensitivity and the expression level of each prognostic gene in the TCGA cohort.

References

[1] R. L. Siegel, K. D. Miller, and A. Jemal, "Cancer statistics, 2020," *CA: A Cancer Journal for Clinicians*, vol. 70, no. 1, pp. 7–30, 2020.

[2] W. Chen, R. Zheng, P. D. Baade et al., "Cancer statistics in China, 2015." *CA: A Cancer Journal for Clinicians*, vol. 66, no. 2, pp. 115–132, 2016.

[3] P. Rawla, T. Sunkara, and V. Gaduputi, "Epidemiology of pancreatic cancer: global trends, etiology and risk factors," *World Journal of Oncology*, vol. 10, no. 1, pp. 10–27, 2019.

[4] D. P. Ryan, T. S. Hong, and N. Bardeesy, "Pancreatic adenocarcinoma," *New England Journal of Medicine*, vol. 371, pp. 1039–1049, 2014.

[5] T. Seufferlein, J. B. Bachet, E. Van Cutsem, and P. Rougier, "Pancreatic adenocarcinoma: ESMO–ESDO clinical practice guidelines for diagnosis, treatment and follow-up," *Annals of Oncology*, vol. 23, no. Supplement 7, pp. VII33–VII40, 2012.

[6] T. Conroy, J.-B. Bachet, A. Ayav et al., "Current standards and new innovative approaches for treatment of pancreatic cancer," *European Journal of Cancer*, vol. 57, pp. 10–22, 2016.

[7] T. Kamisawa, L. D. Wood, T. Itoi, and K. Takaori, "Pancreatic cancer," *The Lancet*, vol. 388, no. 10039, pp. 73–85, 2016.

[8] D. D. Von Hoff, T. Ervin, F. P. Arena et al., "Increased survival in pancreatic cancer with nab-paclitaxel plus gemcitabine," *New England Journal of Medicine*, vol. 369, pp. 1691–1703, 2013.

[9] T. Conroy, Fçoise Desseigne, M. Ychou et al., "FOLFIRINOX versus gemcitabine for metastatic pancreatic cancer," *New England Journal of Medicine*, vol. 364, no. 19, pp. 1817–1825, 2011.

[10] A. Henriksen, A. Dyhl-Polk, I. Chen, and D. Nielsen, "Checkpoint inhibitors in pancreatic cancer," *Cancer Treatment Reviews*, vol. 78, pp. 17–30, 2019.

[11] S. Das, B. Shapiro, E. A. Vucic, S. Vogt, and D. Bar-Sagi, "Tumor cell-derived IL1β promotes desmoplasia and immune suppression in pancreatic cancer," *Cancer Research*, vol. 80, no. 5, pp. 1088–1101, 2020.

[12] S. Bedoui, M. J. Herold, and A. Strasser, "Emerging connectivity of programmed cell death pathways and its physiological implications," *Nature Reviews Molecular Cell Biology*, vol. 21, no. 11, pp. 678–695, 2020.

[13] L. Bai, X. Mei, Y. Wang et al., "The role of netrin-1 in improving functional recovery through autophagy stimulation following spinal cord injury in rats," *Frontiers in Cellular Neuroscience*, vol. 11, Article ID 350, 2017.

[14] L. Li, M. Jiang, L. Qi et al., "Pyroptosis, a new bridge to tumor immunity," *Cancer Science*, vol. 112, no. 10, pp. 3979–3994, 2021.

[15] A. M. Friedlander, "Macrophages are sensitive to anthrax lethal toxin through an acid-dependent process," *Journal of Biological Chemistry*, vol. 261, no. 16, pp. 7123–7126, 1986.

[16] B. T. Cookson and M. A. Brennan, "Pro-inflammatory programmed cell death," *Trends in Microbiology*, vol. 9, no. 3, pp. 113-114, 2001.

[17] L. Galluzzi, I. Vitale, S. A. Aaronson et al., "Molecular mechanisms of cell death: recommendations of the Nomenclature Committee on Cell Death 2018," *Cell Death & Differentiation*, vol. 25, no. 3, pp. 486–541, 2018.

[18] Y. Tan, Q. Chen, X. Li et al., "Pyroptosis: a new paradigm of cell death for fighting against cancer," *Journal of Experimental & Clinical Cancer Research*, vol. 40, no. 1, Article ID 153, 2021.

[19] Y. He, H. Hara, and G. Núñez, "Mechanism and regulation of NLRP3 inflammasome activation," *Trends in Biochemical Sciences*, vol. 41, no. 12, pp. 1012–1021, 2016.

[20] H. Guo, J. B. Callaway, and J. P.-Y. Ting, "Inflammasomes: mechanism of action, role in disease, and therapeutics," *Nature Medicine*, vol. 21, no. 7, pp. 677–687, 2015.

[21] E. Latz, T. S. Xiao, and A. Stutz, "Activation and regulation of the inflammasomes," *Nature Reviews Immunology*, vol. 13, no. 6, pp. 397–411, 2013.

[22] C. A. Lacey, W. J. Mitchell, A. S. Dadelahi, J. A. Skyberg, and G. H. Palmer, "Caspase-1 and caspase-11 mediate pyroptosis, inflammation, and control of brucella joint infection," *Infection and Immunity*, vol. 86, no. 9, 2018.

[23] J. Shi, Y. Zhao, Y. Wang et al., "Inflammatory caspases are innate immune receptors for intracellular LPS," *Nature*, vol. 514, pp. 187–192, 2014.

[24] N. Kayagaki, Søren Warming, M. Lamkanfi et al., "Non-canonical inflammasome activation targets caspase-11," *Nature*, vol. 479, pp. 117–121, 2011.

[25] E. Viganò, C. E. Diamond, R. Spreafico, A. Balachander, R. M. Sobota, and A. Mortellaro, "Human caspase-4 and caspase-5 regulate the one-step non-canonical inflammasome activation in monocytes," *Nature Communications*, vol. 6, no. 1, Article ID 8761, 2015.

[26] K. Wang, Q. Sun, X. Zhong et al., "Structural mechanism for GSDMD targeting by autoprocessed caspases in pyroptosis," *Cell*, vol. 180, no. 5, pp. 941–955.e20, 2020.

[27] S. Rühl and P. Broz, "Caspase-11 activates a canonical NLRP3 inflammasome by promoting K$^+$ efflux," *European Journal of Immunology*, vol. 45, no. 10, pp. 2927–2936, 2015.

[28] N. Kayagaki, I. B. Stowe, B. L. Lee et al., "Caspase-11 cleaves gasdermin D for non-canonical inflammasome signalling," *Nature*, vol. 526, pp. 666–671, 2015.

[29] Y. Wang, W. Gao, X. Shi et al., "Chemotherapy drugs induce pyroptosis through caspase-3 cleavage of a gasdermin," *Nature*, vol. 547, pp. 99–103, 2017.

[30] J. Yu, S. Li, J. Qi et al., "Cleavage of GSDME by caspase-3 determines lobaplatin-induced pyroptosis in colon cancer cells," *Cell Death & Disease*, vol. 10, no. 3, Article ID 193, 2019.

[31] Z. Zhang, Y. Zhang, S. Xia et al., "Gasdermin E suppresses tumour growth by activating anti-tumour immunity," *Nature*, vol. 579, pp. 415–420, 2020.

[32] Y. Liu, Y. Fang, X. Chen et al., "Gasdermin E–mediated target cell pyroptosis by CAR T cells triggers cytokine release syndrome," *Science Immunology*, vol. 5, Article ID eaax7969, 2020.

[33] A. Al Mamun, A. A. Mimi, M. A. Aziz et al., "Role of pyroptosis in cancer and its therapeutic regulation," *European Journal of Pharmacology*, vol. 910, Article ID 174444, 2021.

[34] J. Hou, J.-M. Hsu, and M.-C. Hung, "Molecular mechanisms and functions of pyroptosis in inflammation and antitumor immunity," *Molecular Cell*, vol. 81, no. 22, pp. 4579–4590, 2021.

[35] Z. Chen, Y. Zou, Y. Zhang et al., "A pyroptosis-based prognostic model for immune microenvironment estimation of hepatocellular carcinoma," *Disease Markers*, vol. 2022, Article ID 8109771, 17 pages, 2022.

[36] Z. Dong, L. Bian, M. Wang, L. Wang, and Y. Wang, "Identification of a pyroptosis-related gene signature for prediction of overall survival in lung adenocarcinoma," *Journal of Oncology*, vol. 2021, Article ID 6365459, 15 pages, 2021.

[37] J. Fu and Y. Wang, "Identification of a novel pyroptosis-related gene signature for predicting prognosis in bladder cancer," *Cancer Investigation*, vol. 40, no. 2, pp. 134–150, 2022.

[38] M. J. Goldman, B. Craft, M. Hastie et al., "Visualizing and interpreting cancer genomics data via the Xena platform," *Nature Biotechnology*, vol. 38, no. 6, pp. 675–678, 2020.

[39] Bo Li, Victor Ruotti, Ron M. Stewart, James A. Thomson, and Colin N. Dewey, "RNA-seq gene expression estimation with read mapping uncertainty," *Bioinformatics*, vol. 26, no. 4, pp. 493–500, 2010.

[40] G. P. Wagner, K. Kin, and V. J. Lynch, "Measurement of mRNA abundance using RNA-seq data: RPKM measure is inconsistent among samples," *Theory in Biosciences*, vol. 131, pp. 281–285, 2012.

[41] Y. Ye, Q. Dai, and H. Qi, "A novel defined pyroptosis-related gene signature for predicting the prognosis of ovarian cancer," *Cell Death Discovery*, vol. 7, Article ID 71, 2021.

[42] A. Liberzon, C. Birger, H. Thorvaldsdóttir, M. Ghandi, J. P. Mesirov, and P. Tamayo, "The molecular signatures database hallmark gene set collection," *Cell Systems*, vol. 1, no. 6, pp. 417–425, 2015.

[43] D. Szklarczyk, A. Franceschini, M. Kuhn et al., "The STRING database in 2011: functional interaction networks of proteins, globally integrated and scored," *Nucleic Acids Research*, vol. 39, no. suppl_1, pp. D561–D568, 2010.

[44] X. Zhang, H. Ma, Q. Zou, and J. Wu, "Analysis of cyclin-dependent kinase 1 as an independent prognostic factor for

gastric cancer based on statistical methods," *Frontiers in Cell and Developmental Biology*, vol. 8, Article ID 620164, 2020.

[45] D. Aran, A. Lasry, A. Zinger et al., "Widespread parainflammation in human cancer," *Genome Biology*, vol. 17, no. 1, Article ID 145, 2016.

[46] S. Hänzelmann, R. Castelo, and J. Guinney, "GSVA: gene set variation analysis for microarray and RNA-seq data," *BMC Bioinformatics*, vol. 14, Article ID 7, 2013.

[47] T. Li, J. Fu, Z. Zeng et al., "TIMER2.0 for analysis of tumor-infiltrating immune cells," *Nucleic Acids Research*, vol. 48, no. W1, pp. W509–W514, 2020.

[48] Y. He, Z. Jiang, C. Chen, and X. Wang, "Classification of triple-negative breast cancers based on immunogenomic profiling," *Journal of Experimental & Clinical Cancer Research*, vol. 37, Article ID 327, 2018.

[49] V. Thorsson, D. L. Gibbs, S. D. Brown et al., "The immune landscape of cancer," *Immunity*, vol. 48, no. 4, pp. 812–830. e14, 2018.

[50] P. Geeleher, N. Cox, and R. S. Huang, "pRRophetic: an R package for prediction of clinical chemotherapeutic response from tumor gene expression levels," *PLOS ONE*, vol. 9, no. 9, Article ID e107468, 2014.

[51] W. C. Reinhold, M. Sunshine, H. Liu et al., "CellMiner: a web-based suite of genomic and pharmacologic tools to explore transcript and drug patterns in the NCI-60 cell line set," *Cancer Research*, vol. 72, no. 14, pp. 3499–3511, 2012.

[52] A. Colaprico, T. C. Silva, C. Olsen et al., "TCGAbiolinks: an R/Bioconductor package for integrative analysis of TCGA data," *Nucleic Acids Research*, vol. 44, no. 8, pp. e71–e71, 2016.

[53] W. Roh, P.-L. Chen, A. Reuben et al., "Integrated molecular analysis of tumor biopsies on sequential CTLA-4 and PD-1 blockade reveals markers of response and resistance," *Science Translational Medicine*, vol. 9, no. 379, Article ID eaah3560, 2017.

[54] Y. Hoshida, J.-P. Brunet, P. Tamayo, T. R. Golub, J. P. Mesirov, and O. Hofmann, "Subclass mapping: identifying common subtypes in independent disease data sets," *PLOS ONE*, vol. 2, no. 11, Article ID e1195, 2007.

[55] X. Lu, L. Jiang, L. Zhang et al., "Immune signature-based subtypes of cervical squamous cell carcinoma tightly associated with human papillomavirus type 16 expression, molecular features, and clinical outcome," *Neoplasia*, vol. 21, no. 6, pp. 591–601, 2019.

[56] Z. R. Chalmers, C. F. Connelly, D. Fabrizio et al., "Analysis of 100,000 human cancer genomes reveals the landscape of tumor mutational burden," *Genome Medicine*, vol. 9, Article ID 34, 2017.

[57] S.-K. Hsu, C.-Y. Li, I.-L. Lin et al., "Inflammation-related pyroptosis, a novel programmed cell death pathway, and its crosstalk with immune therapy in cancer treatment," *Theranostics*, vol. 11, no. 18, pp. 8813–8835, 2021.

[58] X. Lu, T. Guo, and X. Zhang, "Pyroptosis in cancer: friend or foe?" *Cancers*, vol. 13, no. 14, Article ID 3620, 2021.

[59] R. W. Birkinshaw, S. Iyer, D. Lio et al., "Structure of detergent-activated BAK dimers derived from the inert monomer," *Molecular Cell*, vol. 81, no. 10, pp. 2123–2134. e5, 2021.

[60] K. Cosentino and A. J. García-Sáez, "Bax and Bak pores: are we closing the circle?" *Trends in Cell Biology*, vol. 27, no. 4, pp. 266–275, 2017.

[61] A. Peña-Blanco and A. J. García-Sáez, "Bax, Bak and beyond—mitochondrial performance in apoptosis," *The FEBS Journal*, vol. 285, no. 3, pp. 416–431, 2018.

[62] K. Tsuchiya, "Switching from apoptosis to pyroptosis: gasdermin-elicited inflammation and antitumor immunity," *International Journal of Molecular Sciences*, vol. 22, no. 1, Article ID 426, 2021.

[63] J. D. Evans, P. A. Cornford, A. Dodson, W. Greenhalf, C. S. Foster, and J. P. Neoptolemos, "Detailed tissue expression of bcl-2, bax, bak and bcl-x in the normal human pancreas and in chronic pancreatitis, ampullary and pancreatic ductal adenocarcinomas," *Pancreatology*, vol. 1, no. 3, pp. 254–262, 2001.

[64] H. Graber, "Bak expression and cell death occur in peritumorous tissue but not in pancreatic cancer cells," *Journal of Gastrointestinal Surgery*, vol. 3, no. 1, pp. 74–81, 1999.

[65] M. Miguchi, T. Hinoi, M. Shimomura et al., "Gasdermin C is upregulated by inactivation of transforming growth factor β receptor type II in the presence of mutated *Apc*, promoting colorectal cancer proliferation," *PLOS ONE*, vol. 11, no. 11, Article ID e0166422, 2016.

[66] K. Watabe, A. Ito, H. Asada et al., "Structure, expression and chromosome mapping of MLZE, a novel gene which is preferentially expressed in metastatic melanoma cells," *Japanese Journal of Cancer Research*, vol. 92, no. 2, pp. 140–151, 2001.

[67] X. Xia, Y. Yu, H. Yang et al., "Gasdermin C as a potential prognostic biomarker and its correlation with immune infiltration in pancreatic ductal adenocarcinoma," *Journal of Clinical Oncology*, vol. 39, no. 15_suppl, Article ID e16256, 2021.

[68] J. Hou, R. Zhao, W. Xia et al., "PD-L1-mediated gasdermin C expression switches apoptosis to pyroptosis in cancer cells and facilitates tumour necrosis," *Nature Cell Biology*, vol. 22, no. 10, pp. 1264–1275, 2020.

[69] S.-T. Wu, G.-H. Sun, C.-Y. Hsu et al., "Tumor necrosis factor-α induces epithelial–mesenchymal transition of renal cell carcinoma cells via a nuclear factor kappa B-independent mechanism," *Experimental Biology and Medicine*, vol. 236, no. 9, pp. 1022–1029, 2011.

[70] J. Wei, Z. Xu, X. Chen et al., "Overexpression of GSDMC is a prognostic factor for predicting a poor outcome in lung adenocarcinoma." *Molecular Medicine Reports*, vol. 21, no. 1, pp. 360–370, 2020.

[71] Y.-Q. Cui, F. Meng, W.-L. Zhan, Z.-T. Dai, and X. Liao, "High expression of GSDMC is associated with poor survival in kidney clear cell cancer," *BioMed Research International*, vol. 2021, Article ID 5282894, 10 pages, 2021.

[72] C. A. Dinarello, D. Novick, S. Kim, and G. Kaplanski, "Interleukin-18 and IL-18 binding protein," *Frontiers in Immunology*, vol. 4, Article ID 289, 2013.

[73] C. A. Dinarello, D. Novick, A. J. Puren et al., "Overview of interleukin-18: more than an interferon-γ inducing factor," *Journal of Leukocyte Biology*, vol. 63, no. 6, pp. 658–664, 1998.

[74] S. Srivastava, N. Salim, and M. J. Robertson, "Interleukin-18: biology and role in the immunotherapy of cancer," *Current Medicinal Chemistry*, vol. 17, no. 29, pp. 3353–3357, 2010.

[75] K.-E. Kim, H. Song, T. S. Kim et al., "Interleukin-18 is a critical factor for vascular endothelial growth factor-enhanced migration in human gastric cancer cell lines," *Oncogene*, vol. 26, no. 10, pp. 1468–1476, 2007.

[76] B. Zhang, K.-F. Wu, Z.-Y. Cao et al., "IL-18 increases invasiveness of HL-60 myeloid leukemia cells: up-regulation of matrix metalloproteinases-9 (MMP-9) expression," *Leukemia Research*, vol. 28, no. 1, pp. 91–95, 2004.

[77] Y. Zhao, M. Shen, Y. Feng et al., "Regulatory B cells induced by pancreatic cancer cell-derived interleukin-18 promote immune tolerance via the PD-1/PD-L1 pathway," *Oncotarget*, vol. 9, no. 19, pp. 14803–14814, 2018.

[78] X. Guo, L. Zheng, J. Jiang et al., "Blocking NF-κB is essential for the immunotherapeutic effect of recombinant IL18 in pancreatic cancer," *Clinical Cancer Research*, vol. 22, no. 23, pp. 5939–5950, 2016.

[79] A. Carbone, B. Vizio, A. Novarino et al., "IL-18 paradox in pancreatic carcinoma: elevated serum levels of free IL-18 are correlated with poor survival," *Journal of Immunotherapy*, vol. 32, no. 9, pp. 920–931, 2009.

[80] C. J. McKay, P. Glen, and D. C. McMillan, "Chronic inflammation and pancreatic cancer," *Best Practice & Research Clinical Gastroenterology*, vol. 22, no. 1, pp. 65–73, 2008.

[81] S.-H. Kim, M. Eisenstein, L. Reznikov et al., "Structural requirements of six naturally occurring isoforms of the IL-18 binding protein to inhibit IL-18," *Proceedings of the National Academy of Sciences*, vol. 97, no. 3, pp. 1190–1195, 2000.

[82] R. Medzhitov, "Origin and physiological roles of inflammation," *Nature*, vol. 454, pp. 428–435, 2008.

[83] A. Pribluda, E. Elyada, Z. Wiener et al., "A senescence-inflammatory switch from cancer-inhibitory to cancer-promoting mechanism," *Cancer Cell*, vol. 24, no. 2, pp. 242–256, 2013.

[84] K. A. Smith, G. B. Waypa, and P. T. Schumacker, "Redox signaling during hypoxia in mammalian cells," *Redox Biology*, vol. 13, pp. 228–234, 2017.

[85] P. Vaupel and A. Mayer, "Hypoxia in cancer: significance and impact on clinical outcome," *Cancer and Metastasis Reviews*, vol. 26, pp. 225–239, 2007.

[86] L. Galluzzi and C. Vanpouille-Box, "BAX and BAK at the gates of innate immunity," *Trends in Cell Biology*, vol. 28, no. 5, pp. 343–345, 2018.

[87] C. Vanpouille-Box, S. Demaria, S. C. Formenti, and L. Galluzzi, "Cytosolic DNA sensing in organismal tumor control," *Cancer Cell*, vol. 34, no. 3, pp. 361–378, 2018.

[88] A. Blaauboer, K. Sideras, C. H. J. van Eijck, and L. J. Hofland, "Type I interferons in pancreatic cancer and development of new therapeutic approaches," *Critical Reviews in Oncology/Hematology*, vol. 159, Article ID 103204, 2021.

[89] S. M. Man, R. Karki, R. K. S. Malireddi et al., "The transcription factor IRF1 and guanylate-binding proteins target activation of the AIM2 inflammasome by Francisella infection," *Nature Immunology*, vol. 16, pp. 467–475, 2015.

[90] M. Zheng and T-Devi Kanneganti, "The regulation of the ZBP1-NLRP3 inflammasome and its implications in pyroptosis, apoptosis, and necroptosis (PANoptosis)," *Immunological Reviews*, vol. 297, no. 1, pp. 26–38, 2020.

[91] T. Kuriakose, S. M. Man, R. K. Subbarao Malireddi et al., "ZBP1/DAI is an innate sensor of influenza virus triggering the NLRP3 inflammasome and programmed cell death pathways," *Science Immunology*, vol. 1, no. 2, Article ID aag2045, 2016.

[92] W. Xiao, J. D. Klement, C. Lu, M. L. Ibrahim, and K. Liu, "IFNAR1 controls autocrine type I IFN regulation of PD-L1 expression in myeloid-derived suppressor cells," *The Journal of Immunology*, vol. 201, no. 1, pp. 264–277, 2018.

[93] A. Sharma, J. F. Arambula, S. Koo et al., "Hypoxia-targeted drug delivery," *Chemical Society Reviews*, vol. 48, no. 3, pp. 771–813, 2019.

[94] G.-Y. Liou, H. Döppler, B. Necela et al., "Mutant KRAS-induced expression of ICAM-1 in pancreatic acinar cells causes attraction of macrophages to expedite the formation of precancerous lesions," *Cancer Discovery*, vol. 5, no. 1, pp. 52–63, 2015.

[95] M. Budhwani, R. Mazzieri, and R. Dolcetti, "Plasticity of type I interferon-mediated responses in cancer therapy: from antitumor immunity to resistance," *Frontiers in Oncology*, vol. 8, Article ID 322, 2018.

[96] G. P. Dunn, C. M. Koebel, and R. D. Schreiber, "Interferons, immunity and cancer immunoediting," *Nature Reviews Immunology*, vol. 6, no. 11, pp. 836–848, 2006.

[97] R. Yu, B. Zhu, and D. Chen, "Type I interferon-mediated tumor immunity and its role in immunotherapy," *Cellular and Molecular Life Sciences*, vol. 79, no. 3, Article ID 191, 2022.

[98] M. Collin and V. Bigley, "Human dendritic cell subsets: an update," *Immunology*, vol. 154, no. 1, pp. 3–20, 2018.

[99] S. L. Jongbloed, A. J. Kassianos, K. J. McDonald et al., "Human CD141⁺ (BDCA-3)⁺ dendritic cells (DCs) represent a unique myeloid DC subset that cross-presents necrotic cell antigens," *Journal of Experimental Medicine*, vol. 207, no. 6, pp. 1247–1260, 2010.

[100] L. M. Snell, T. L. McGaha, and D. G. Brooks, "Type I interferon in chronic virus infection and cancer," *Trends in Immunology*, vol. 38, no. 8, pp. 542–557, 2017.

[101] J. L. Benci, B. Xu, Y. Qiu et al., "Tumor interferon signaling regulates a multigenic resistance program to immune checkpoint blockade," *Cell*, vol. 167, no. 6, pp. 1540–1554. E12, 2016.

[102] L. Zhou, Y. Zhang, Y. Wang et al., "A dual role of type I interferons in antitumor immunity," *Advanced Biosystems*, vol. 4, no. 11, Article ID 1900237, 2020.

[103] D. Marvel and D. I. Gabrilovich, "Myeloid-derived suppressor cells in the tumor microenvironment: expect the unexpected," *Journal of Clinical Investigation*, vol. 125, no. 9, pp. 3356–3364, 2015.

[104] A. Thyagarajan, M. S. A. Alshehri, K. L. R. Miller, C. M. Sherwin, J. B. Travers, and R. P. Sahu, "Myeloid-derived suppressor cells and pancreatic cancer: implications in novel therapeutic approaches," *Cancers*, vol. 11, no. 11, Article ID 1627, 2019.

[105] D. I. Gabrilovich, "Myeloid-derived suppressor cells," *Cancer Immunology Research*, vol. 5, no. 1, pp. 3–8, 2017.

[106] D. Bausch, T. Pausch, T. Krauss et al., "Neutrophil granulocyte derived MMP-9 is a VEGF independent functional component of the angiogenic switch in pancreatic ductal adenocarcinoma," *Angiogenesis*, vol. 14, pp. 235–243, 2011.

[107] T. Große-Steffen, T. Giese, N. Giese et al., "Epithelial-to-mesenchymal transition in pancreatic ductal adenocarcinoma and pancreatic tumor cell lines: the role of neutrophils and neutrophil-derived elastase," *Clinical and Developmental Immunology*, vol. 2012, Article ID 720768, 12 pages, 2012.

[108] N. Pu, H. Yin, G. Zhao et al., "Independent effect of postoperative neutrophil-to-lymphocyte ratio on the survival of pancreatic ductal adenocarcinoma with open distal pancreatosplenectomy and its nomogram-based prediction," *Journal of Cancer*, vol. 10, no. 24, pp. 5935–5943, 2019.

[109] Q. Ben, W. An, L. Wang, W. Wang, L. Yu, and Y. Yuan, "Validation of the pretreatment neutrophil-lymphocyte ratio as a predictor of overall survival in a cohort of patients with pancreatic ductal adenocarcinoma," *Pancreas*, vol. 44, no. 3, pp. 471–477, 2015.

[110] Y. Yi, H.-W. He, J.-X. Wang et al., "The functional impairment of HCC-infiltrating γδ T cells, partially mediated by regulatory T

cells in a TGFβ-and IL-10-dependent manner," *Journal of Hepatology*, vol. 58, no. 5, pp. 977–983, 2013.

[111] Y. Tang, X. Xu, S. Guo et al., "An increased abundance of tumor-infiltrating regulatory T cells is correlated with the progression and prognosis of pancreatic ductal adenocarcinoma," *PLOS ONE*, vol. 9, no. 3, Article ID e91551, 2014.

[112] L. De Monte, M. Reni, E. Tassi et al., "Intratumor T helper type 2 cell infiltrate correlates with cancer-associated fibroblast thymic stromal lymphopoietin production and reduced survival in pancreatic cancer," *Journal of Experimental Medicine*, vol. 208, no. 3, pp. 469–478, 2011.

[113] E. Bolli, K. Movahedi, D. Laoui, and J. A. Van Ginderachter, "Novel insights in the regulation and function of macrophages in the tumor microenvironment," *Current Opinion in Oncology*, vol. 29, no. 1, pp. 55–61, 2017.

[114] H. Hu, J.-J. Hang, T. Han, M. Zhuo, F. Jiao, and L.-W. Wang, "The M2 phenotype of tumor-associated macrophages in the stroma confers a poor prognosis in pancreatic cancer," *Tumor Biology*, vol. 37, pp. 8657–8664, 2016.

[115] D. von Ahrens, T. D. Bhagat, D. Nagrath, A. Maitra, and A. Verma, "The role of stromal cancer-associated fibroblasts in pancreatic cancer," *Journal of Hematology & Oncology*, vol. 10, Article ID 76, 2017.

[116] E. Sahai, I. Astsaturov, E. Cukierman et al., "A framework for advancing our understanding of cancer-associated fibroblasts," *Nature Reviews Cancer*, vol. 20, pp. 174–186, 2020.

[117] X. Geng, H. Chen, L. Zhao et al., "Cancer-associated fibroblast (CAF) heterogeneity and targeting therapy of CAFs in pancreatic cancer," *Frontiers in Cell and Developmental Biology*, vol. 9, Article ID 655152, 2021.

[118] J. Wu, Y. Wang, and Z. Jiang, "TNFSF9 is a prognostic biomarker and correlated with immune infiltrates in pancreatic cancer," *Journal of Gastrointestinal Cancer*, vol. 52, pp. 150–159, 2021.

[119] X. Zhao, D.-C. Li, X.-G. Zhu et al., "B7-H3 overexpression in pancreatic cancer promotes tumor progression," *International Journal of Molecular Medicine*, vol. 31, no. 2, pp. 283–291, 2013.

[120] F. Wang, G. Wang, T. Liu, G. Yu, G. Zhang, and X. Luan, "Xiying Luan, B7-H3 was highly expressed in human primary hepatocellular carcinoma and promoted tumor progression," *Cancer Investigation*, vol. 32, no. 6, pp. 262–271, 2014.

[121] Y. Mao, L. Chen, F. Wang et al., "Cancer cell-expressed B7-H3 regulates the differentiation of tumor-associated macrophages in human colorectal carcinoma," *Oncology Letters*, vol. 14, no. 5, pp. 6177–6183, 2017.

[122] W. Zou and L. Chen, "Inhibitory B7-family molecules in the tumour microenvironment," *Nature Reviews Immunology*, vol. 8, pp. 467–477, 2008.

[123] X. Wang, F. Teng, and L. Kong, "PD-L1 expression in human cancers and its association with clinical outcomes," *OncoTargets and Therapy*, vol. 9, pp. 5023–5039, 2016.

[124] T. Nomi, M. Sho, T. Akahori et al., "Clinical significance and therapeutic potential of the programmed death-1 ligand/programmed death-1 pathway in human pancreatic cancer," *Clinical Cancer Research*, vol. 13, no. 7, pp. 2151–2157, 2007.

[125] S. P. Patel and R. Kurzrock, "PD-L1 expression as a predictive biomarker in cancer immunotherapy," *Molecular Cancer Therapeutics*, vol. 14, no. 4, pp. 847–856, 2015.

[126] L. Wang, Q. Ma, X. Chen, K. Guo, J. Li, and M. Zhang, "Clinical significance of B7-H1 and B7-1 expressions in pancreatic carcinoma," *World Journal of Surgery*, vol. 34, pp. 1059–1065, 2010.

[127] L. Geng, D. Huang, J. Liu et al., "B7-H1 up-regulated expression in human pancreatic carcinoma tissue associates with tumor progression," *Journal of Cancer Research and Clinical Oncology*, vol. 134, pp. 1021–1027, 2008.

[128] S. Bansod, P. B. Dodhiawala, and K.-H. Lim, "Oncogenic KRAS-induced feedback inflammatory signaling in pancreatic cancer: an overview and new therapeutic opportunities," *Cancers*, vol. 13, no. 21, Article ID 5481, 2021.

[129] S. M. Wörmann, L. Song, J. Ai et al., "Loss of P53 function activates JAK2-STAT3 signaling to promote pancreatic tumor growth, stroma modification, and gemcitabine resistance in mice and is associated with patient survival," *Gastroenterology*, vol. 151, no. 1, pp. 180–193.E12, 2016.

[130] T. Wang, S. Kong, M. Tao, and S. Ju, "The potential role of RNA N6-methyladenosine in cancer progression," *Molecular Cancer*, vol. 19, Article ID 88, 2020.

[131] Z. Li, Y. Li, W. Zhong, and P. Huang, "m6A-Related lncRNA to develop prognostic signature and predict the immune landscape in bladder cancer." *Journal of Oncology*, vol. 2021, Article ID 7488188, 16 pages, 2021.

[132] X.-T. Huang, J.-H. Li, X.-X. Zhu et al., "HNRNPC impedes m6A-dependent anti-metastatic alternative splicing events in pancreatic ductal adenocarcinoma," *Cancer Letters*, vol. 518, pp. 196–206, 2021.

[133] X. Cai, Y. Chen, D. Man et al., "RBM15 promotes hepatocellular carcinoma progression by regulating N6-methyladenosine modification of YES1 mRNA in an IGF2BP1-dependent manner," *Cell Death Discovery*, vol. 7, Article ID 315, 2021.

[134] X. Wang, L. Tian, Y. Li et al., "RBM15 facilitates laryngeal squamous cell carcinoma progression by regulating TMBIM6 stability through IGF2BP3 dependent," *Journal of Experimental & Clinical Cancer Research*, vol. 40, Article ID 80, 2021.

[135] D. Han, J. Liu, C. Chen et al., "Anti-tumour immunity controlled through mRNA m6A methylation and YTHDF1 in dendritic cells," *Nature*, vol. 566, pp. 270–274, 2019.

[136] D. J. Kim and A. Iwasaki, "YTHDF1 control of dendritic cell cross-priming as a possible target of cancer immunotherapy," *Biochemistry*, vol. 58, no. 15, pp. 1945-1946, 2019.

[137] T. Liu, Q. Wei, J. Jin et al., "The m6A reader YTHDF1 promotes ovarian cancer progression via augmenting EIF3C translation," *Nucleic Acids Research*, vol. 48, no. 7, pp. 3816–3831, 2020.

[138] L. Liu, X. Liu, Z. Dong et al., "N6-methyladenosine-related genomic targets are altered in breast cancer tissue and associated with poor survival," *Journal of Cancer*, vol. 10, no. 22, pp. 5447–5459, 2019.

[139] X. Guo, K. Li, W. Jiang et al., "RNA demethylase ALKBH5 prevents pancreatic cancer progression by posttranscriptional activation of PER1 in an m6A-YTHDF2-dependent manner," *Molecular Cancer*, vol. 19, Article ID 91, 2020.

[140] S. L. Topalian, J. M. Taube, R. A. Anders, and D. M. Pardoll, "Mechanism-driven biomarkers to guide immune checkpoint blockade in cancer therapy," *Nature Reviews Cancer*, vol. 16, no. 5, pp. 275–287, 2016.

[141] K. Ganesh, Z. K. Stadler, A. Cercek et al., "Immunotherapy in colorectal cancer: rationale, challenges and potential," *Nature Reviews Gastroenterology & Hepatology*, vol. 16, no. 6, pp. 361–375, 2019.

[142] S. Lemery, P. Keegan, and R. Pazdur, "First FDA approval agnostic of cancer site—when a biomarker defines the indication," *New England Journal of Medicine*, vol. 377, no. 15, pp. 1409–1412, 2017.